Journal of Minerals and Materials Characterization and Engineering, 2025, 13(6), 328-369
https://www.scirp.org/journal/jmmce
ISSN Online: 2327-4085
ISSN Print: 2327-4077

Formulation and Investigation of Thermo Mechanical Properties of a Friction Material (Liner) Made from Ox Horn Particles

Moungnutou Ndam Soulemanou[1], Anyi Joseph Nkongho[1,2,3*], Theodore Tchotang[1], Mahonde[1]

[1]Department of Mechanical Engineering, National Advanced School of Engineering of Yaoundé, University of Yaoundé I, Yaoundé, Cameroon
[2]Department of Mechanical Engineering, Higher Technical Teachers Training College, University of Buea in Kumba, Kumba, Cameroon
[3]Laboratory of Mechanics and Material (LMEMA), National Advanced school of Engineering of Douala, Universdy of Douala, Douala, Cameroon
Email: *nkongho.anyi@ubuea.cm

How to cite this paper: Soulemanou, M.N., Nkongho, A.J., Tchotang, T. and Mahonde (2025) Formulation and Investigation of Thermo Mechanical Properties of a Friction Material (Liner) Made from Ox Horn Particles. *Journal of Minerals and Materials Characterization and Engineering*, **13**, 328-369.
https://doi.org/10.4236/jmmce.2025.136019

Received: August 10, 2025
Accepted: November 11, 2025
Published: November 14, 2025

Abstract

This article investigates into the physical and thermo mechanical properties of a friction composite material based on ox horn and phenolic resin. The tests revealed that an intermediate density of 100 µm offers a good balance between density and homogeneity. Increasing the horn particles fraction reduces the density of the composite, thereby influencing its compactness and porosity. Scanning electron microscopy (SEM) and transmission electron microscopy (TEM) morphology analysis revealed that fine particles (50 µm) provide good dispersion and promote porosity. Intermediate particles (100 µm) offer the best balance of cohesion, low porosity and good mechanical performance. Coarse particles (300 µm) provide greater density but less effective interfacial adhesion. The compressive strength of the composite depends heavily on particle size and horn particles fraction. The static friction coefficient of the horn particles and phenolic resin composite (100 µm) is 0.42/0.35 (for Kevlar-based brake linings) and 0.40 (for carbon fibre-based linings). Wear tests have proven that the ox horn and phenolic resin composite varies between 2.5 - 3.0 (mm^3/Nm) and 1.5 - 2.0 (mm^3/Nm).

Keywords

Investigation, Friction Material, Horns Particles, Thermal Properties, Mechanical Properties

1. Introduction

A composite material is an assembly of at least two immiscible materials of different and complementary natures that have strong adhesion properties, giving rise to a new heterogeneous material with better performance characteristics than other commonly used materials [1]. Due to their high performance (excellent mechanical resistance and low density), composites have gradually replaced conventional materials. The reinforcement of natural filler materials in the composite matrix increases the modulus and decreases the ductility of the matrix, as well as reducing the cost of composites. Naturally filled polymer composites have many industrial applications and offer better mechanical and tribology properties than synthetic material composites [2] [3]. Researchers have investigated the potential of natural fillers as composite reinforcements. Polymer-based composites are becoming an essential part of today's materials, successfully replacing traditional materials in applications requiring a high strength-to-weight ratio, high tensile strength, high temperature resistance, high creep resistance, high toughness, low weight, a good surface finish and low cost [4] [5]. The compositional characteristics of bovine horn sheaths have been studied in previous literature. The linear viscoelasticity of gemsbok horn sheaths and the effect of water have also been studied [6]. The fracture toughness of gemsbok (Oryx gazella), mouflon (Ovis Aries musimon) and waterbuck (Kobus ellipsiprymnus) horn sheaths has been systematically measured as a function of water content. Interestingly, the results have been applied to understanding horn behaviour [7] [8]. The dielectric properties of horn sheaths from calves, cows and rhinoceroses have also been studied [9]. Understanding the mechanical properties of bovine horns can help us to gain a deeper insight into their natural design, adaptation, structure and function. However, it is surprising that little attention has been paid to the mechanical properties of horn sheaths. Pushing and wrestling contests are often observed in domestic cattle [10]. Friction materials are essential for braking and clutch systems, where mechanical and thermal stability, as well as low wear, must be ensured [11]. Among the compounds developed, integrating natural materials such as ox horn particle into a phenolic matrix offers an ecological and economical alternative to traditional composites. Using ox horn as a natural reinforcing particles provides an alternative to synthetic or legislative fibres while offering good mechanical resistance and satisfactory tribological behaviour [12]-[14]. Phenolic resin, on the other hand, is widely used due to its good mechanical and thermal resistance, with a decomposition temperature above 400˚C [15]. This works analysed in detail the physical, mechanical and thermal characteristics of a composite exclusively made of ox horn particles (5% to 25%) and phenolic resin. The main objective is to evaluate the impact of ox horn on the mechanical properties of a resin matrix composite material, particularly with regard to wear resistance, hardness, and compressive strength [16]. The combination of ox horn particles and phenolic resin aims to optimise the tribological and mechanical performance of the material while reducing the environmental impact associated with mineral fibres and synthetic fibres. This friction material

has potential applications in the automotive, railway and aerospace industries, where it could be used in brake pads, clutch facings and other components subject to high friction.

2. Materials and Methods

2.1. Materials

2.1.1. Sample Collection

1) Horns

The horns used in this study came from cattle slaughtered at the municipal slaughterhouse in Douala, Cameroon. They were recovered after slaughter, selected, cleaned, and prepared for use in the formulation of phenolic resin-based composite materials. The animals were mainly adult cattle (local bulls or zebu) aged 3 to 6 years. The horns exhibit the following morphological characteristics (see Table 1). The horns are primarily composed of hard keratin, a sulfur-rich fibrous protein. The base is dense and solid, while the tip is often hollow. The color ranges from brown to black. The outer surface is smooth and abrasion-resistant. To optimize grinding and particle uniformity, the horns were divided into three longitudinally distinct zones. The proximal zone, located at the base near the skull, is very dense and particularly rich in keratin; the middle zone, of moderate density, constitutes an ideal intermediate portion for balanced grinding; finally, the distal zone, finer and sometimes hollow, is often separated in order to limit the heterogeneity of the particles obtained. The horns were carefully washed (see Figure 1(a)), dried at 60˚C for 48 hours (see Figure 1(b)), then ground and sieved (see Figure 1(c) and Figure 1(d)). The particle sizes used for the tests were: 50 µm, 100 µm and 300 µm (see Figures 2(a)-(c)) according to the BS/ISO 3310 standard.

Table 1. Morphological characteristics of the ox horns used.

Measured Parameter	Average value	Range observed
Total Length	25 - 40 cm	22 - 44 cm
Diameter at Base (Head)	5 - 8 cm	4.5 - 9 cm
Diameter at Tip	1 - 2 cm	0.8 - 2.5 cm
Average Mass (Dry)	200 - 300 g	depending on humidity

(a) (b) (c) (d)

Figure 1. Horns processing. (a) Horns soaked in water; (b) Horns separated from the core; (c) and (d) Crushed and separated horns particles of different sizes.

(a) (b) (c)

Figure 2. Ground horns separated into different sizes. (a) 300 µm; (b) 100 µm; (c) 50 µm.

2) Resin

To achieve an optimal composite of ox horn and phenolic resin, the choice of resin is crucial. Here is an analysis of the two main options (Table 2).

Table 2. Comparison of phenolic resins for ox horn composites [17].

Type	Advantages	Disadvantages
Novolac Resin (Thermosetting)	Very good thermal and mechanical stability. Excellent adhesion to ox horn. Low moisture absorption.	- Requires a hardener (e.g., hexamethylenetetramine). - More complex manufacturing process
Resole Resin (self-hardening)	• Easier to mold (self-hardening). • Good compromise between rigidity and elasticity. • Good friction behavior.	- Less thermally stable than Novolac. - Can absorb slightly more moisture

Novolac resin (see Figure 3) is the best choice for a composite of ox horn and phenolic resin because it offers the following advantages: better mechanical strength, high thermal stability and low degradation under friction.

Figure 3. Phenolic resin.

However, Resole resin remains an attractive alternative if easier shaping and lower production costs are desired. The use of phenolic resin requires a hardener to ensure thermal stability.

3) HTM (hexamethylenetetramine) hardener

HMT (hexamethylenetetramine) hardener is used in the horn powder + phe-

nolic novolac resin mixture for several specific reasons related to the chemistry of novolac resins. Phenolic novolac resin is thermoplastic by nature, meaning it does not harden spontaneously under heat. The addition of HMT allows it to become a thermosetting polymer through a crosslinking reaction. This allows for: thermal crosslinking under the influence of heat and pressure; HMT releases formaldehyde, which reacts with the hydroxyl groups of the novolac to form a rigid and thermally stable matrix. Improved mechanical properties: The curing process improves the adhesion between the resin and the horn particles, thus increasing the hardness, strength, and stability of the composite. Chemical compatibility: Horn powder contains functional groups capable of interacting with the cured resin, thus improving adhesion. Controlled curing: HMT allows for controlled curing during molding, thus facilitating the shaping of composite parts. HMT is essential for transforming the novolac resin into a cured network capable of ensuring the rigidity and durability of the composite. It allows the resin to effectively fulfill its role as a matrix in a high-performance composite material.

2.1.2. Composite Formulation Process

1) Humidity of the horn particles

The moisture content of ox horn particles depends on their preparation and drying. Typical values include [18]:

- Fresh (undried) horn: approximately 30% - 40% moisture content;
- Air-dried or oven-dried horn: 5% - 10% moisture content;
- Ground and well-dried horn for industrial or composite applications often has a moisture content below 5% (usually around 2% - 4%) to avoid unwanted reactions with the resin during hot pressing. Different proportions of ox horn particles, novolac phenolic resin, and HMT (hexamethylenetetramine) hardener are used (**Tables 1-3**).

Table 3. Samples with different proportions of particles, novolac resin, and HMT hardener.

Sample	Ox horn (%)	Novolac resin (%)	HMT hardener (%)
Ep5	5	92	3
Ep10	10	87	3
Ep15	15	82	3
Ep20	20	77	3
Ep25	25	72	3

HMT (hexamethylenetetramine) is a crosslinking agent that solidifies the resin. The specimens are molded under pressure and under heat to obtain shapes suitable for mechanical and tribological testing.

2) Mixing the Components

The mixing of the composite material based on ox horn, phenolic resin, and HMT follows a strictly controlled protocol to ensure optimal homogeneity and chemical

reactivity. The ox horn is first ground and dried to obtain a fine powder (<300 μm). The phenolic resin is then dry-mixed with 3% HMT for 10 to 15 minutes to ensure uniform distribution of the hardener. This homogeneous, lump-free mixture is then ready for the molding stage, according to standard procedures (see Figure 4). Mixing resin-ox horn and HMT hardener (see Figure 4(a)); obtaining a homogeneous powder (See Figure 4(b)); hot pressing in a four variable temperatures depending on the formulation (see Figure 4(c)) and obtaining the different shapes for testing (see Figure 4(d)).

Figure 4. Resin-bovine horn mixing (a), homogeneous mixture (b), hot pressing (c), and resulting specimen shapes (d).

Powdered phenolic resin has a light brown to reddish tint, even before heat treatment. This coloration is due to the aromatic groups and conjugated bonds in its chemical structure, characteristic of phenol-formaldehyde-based resins. Although generally colorless or slightly yellowish, HMT can partially react with the resin, even at room temperature, initiating slow pre-crosslinking. This phenomenon can intensify the brownish tint of the mixture at this stage.

3) Mixture Homogenization

The finely powdered components: ox horn (organic filler), phenolic resin (thermosetting binder), and hexamethylenetetramine (HMT, crosslinking agent) are first weighed in predefined proportions and then dry-mixed until a uniform texture is obtained, without visible agglomerates. This homogeneity is essential to ensure uniform crosslinking and cohesion of the material. The mixture is then transferred into a metal mold of defined geometry (usually cylindrical or parallelepiped). Cold compaction is applied under a pressure of between 5 and 10 MPa to perform the material and eliminate initial voids. This step ensures the density and shape of the sample before polymerization. The molded part is subjected to heat treatment in a press heated to a temperature of between 160˚C and 180˚C for 30 to 60 minutes. At this temperature, the phenolic resin undergoes irreversible polymerization, activated by HMT. This thermally induced hardening ensures the strength of the three-dimensional network and gives the material its thermo mechanical properties. After polymerization, the material is allowed to cool gradually to room temperature to avoid thermal shock and cracks. Finally, the samples are machined to standardized dimensions (see Table 4) for mechanical and thermal testing.

Table 4. Different specimen shapes according to tests and dimensions.

Type of specimen	Associated test	Dimensions (mm)
Rectangular	Density, water absorption	50 × 10 × 5
Cylindrical	Compression test	Ø10 × 20
Disc	Tribological test (wear, friction)	Ø40 × 5

2.2. Methods

2.2.1. Physical Characteristics of the Composite

The study of the physical properties of the composite focused on particle size, density, specific surface area, porosity, and particle morphology.

1) Particle size

The particle size distribution of the ox horn powder was determined by dry sieving in accordance with ASTM D422-63 (2007), which describes procedures for the particle size analysis of soils and powdered materials by mechanical means. The method involves passing a known mass of dried sample through a series of sieves with progressively finer mesh sizes, typically from 2 mm to 50 µm or finer, depending on the application.

Each sieve is stacked in descending order of aperture size and mounted on a mechanical shaker. The sample is placed on the upper sieve and subjected to vibration for a set period of time (usually 10 to 15 minutes), allowing particle size separation. The mass retained on each sieve is then weighed, and the mass percentage is calculated relative to the total sample. This allows for the construction of a particle size distribution curve.

This method ensures reproducibility and reliability in assessing the powder's textural properties, which directly influence its behavior during composite formation, including compaction, homogeneity, and interaction with the binder phase.

2) Density of the composite

The density of a composite is calculated using the following formula:

$$\rho_c = \frac{m_1 + m_2}{V}; \tag{1}$$

Considering the densities of the constituents:

$$\rho_c = \rho_f V_f + \rho_m V_m; \tag{2}$$

with ρ_c = Density of the composite (g/cm³), ρ_f = Density of the filler (ox horn) (g/cm³), ρ_m = Density of the matrix (phenolic resin) (g/cm³), V_f = Volume fraction of the particles (cm³), V_m = Volume fraction of the matrix ($V_m = 1 - V_f$).

The average density of ox horn is about 1.2 g/cm³, while that of phenolic resin is between 1.3 and 1.4 g/cm³.

3) Specific surface area

The specific surface area (SSA) of a composite depends on the particle size (ox horn) and their volume fraction. It is generally calculated using the following re-

lationship:

$$S = \frac{6}{d}\frac{V_f}{\rho_f} \tag{3}$$

where: S is the specific surface area (m^2/g); d is the average particle diameter (μm), V_f is the volume fraction of the ox horn, and ρ_f is the density of the ox horn (g/cm^3).

This formula assumes that the particles are spherical and well dispersed in the matrix.

4) Composite density

The mass (ρ) of a composite is determined by the relationship:

$$\rho_{\text{composite}} = \frac{m_{\text{composite}}}{V_{\text{composite}}} \tag{4}$$

Considering a composite composed of ox horn, Novolac phenolic resin and HMT, its density is obtained by the mixture model:

$$\rho_{\text{composite}} = \frac{x_c}{\rho_c} + \frac{x_r}{\rho_r} + \frac{x_h}{\rho_h}. \tag{5}$$

where is the composite density (g/cm^3), are the respective densities of the ox horn particle, phenolic resin and HMT, and then are the mass fractions of each component.

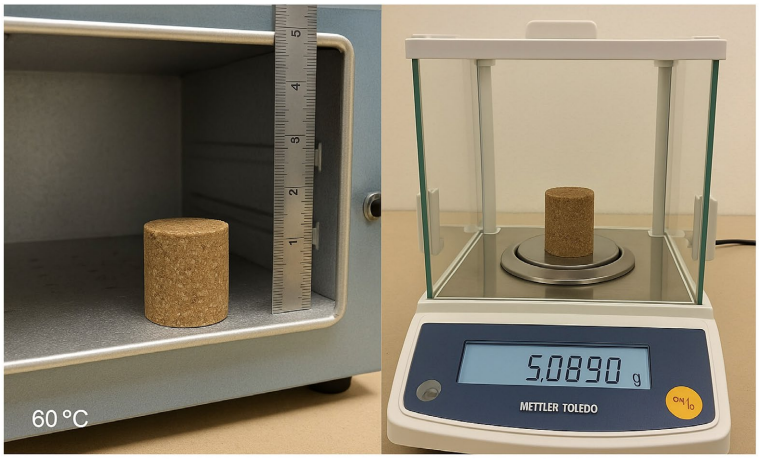

Figure 5. Experimental setup for composite density.

The experimental methodology for density determination and sample weighing was followed. To determine the density of the composite material, standard samples were prepared from ox horn particles of different particle sizes (50 μm, 100 μm, and 300 μm). Each sample was first oven-dried at 60˚C for 24 hours to remove any residual moisture that could affect mass or volume measurements. After drying, the samples were weighed using a high-precision analytical balance, with an accuracy of ±0.0001 g, to ensure reliable mass values (see **Figure 5**).

The volume of each sample was then determined using Archimedes' principle. This method involves immersing the sample in a liquid of known density (usually distilled water) and measuring the volume of fluid displaced. Precautions were taken to avoid the formation of air bubbles and ensure complete immersion. This approach allows for accurate volume determination, especially for irregularly shaped or porous samples. The density was finally calculated using the formula.

$$\rho = \frac{m}{V} \tag{6}$$

where: m is the measured mass, V is the displaced volume, and ρ_{liq} (ethanol, ρ = 0.789 g/cm^3) is the density. Measure the displaced volume V using a pycnometer, then calculate the density as follows:

'erification by Gas Pycnometer (Helium Method)

Figure 6. Gas pycnometer verification setup (helium method).

The gas pycnometer verification (helium method) is performed. The true density of the ceramic samples was determined using a gas pycnometer based on the helium displacement method, widely recognized for its high accuracy due to the small atomic size and inertia of helium (see **Figure 6**). This technique allows the volume of the solid phase alone to be measured, excluding open and closed porosities, and thus allows for accurate assessment of the skeletal density [19] [20].

The gas pycnometer operates according to Boyle's law, which states that the pressure and volume of a gas are inversely proportional at constant temperature. In this method, a known volume of helium is introduced into a sample chamber containing the sample. The gas is then expanded into a reference chamber. By measuring the pressure variation before and after expansion, the volume of the solid sample is calculated. The helium method offers the following advantages: high accuracy and repeatability, non-destructiveness, and minimal adsorption or

interaction with the sample surface, making it ideal for porous and heterogeneous materials such as ceramics.

5) Determination of apparent and true density.

A composite material has a true density (ρ_r), which corresponds to the density of the constituents without taking into account porosities, and an apparent density (ρ_a), which takes into account the voids and porosities present in the material. The true density (ρ_r) is as follows:

$$\rho_r = \frac{m}{V_{reel}}. \tag{7}$$

where: m is the mass of the composite and V_{reel} the total volume of the composite without porosity (volume of horn and resin particles). Furthermore, the apparent density (ρ_a) is as follows:

$$\rho_a = \frac{m}{V_{app}}. \tag{8}$$

where V_{app} is the total volume of the composite, including porosities.

The determination of the true and apparent densities of the composites was carried out using two complementary approaches. For the true density, two methods were used: helium pycnometry, which allows for precise measurement of the material's true volume while taking into account internal porosity, and immersion in a liquid of known density, a reference technique for evaluating porous materials. The apparent density was calculated from the geometric volume of the samples. This volume was determined by measuring the dimensions using a caliper, without taking internal porosity into account. These two measurements allow for a complete characterization of the material, highlighting variations related to its internal structure.

The experimental procedure involved several steps to determine the true and apparent densities of the samples. First, each sample was weighed (m) using a precision balance. Next, its apparent volume (V_{app}) was calculated by measuring the geometric dimensions using a caliper. The true volume (V_{reel}) was determined either using a helium pycnometer or by the Archimedes method, both of which take internal porosity into account. Finally, the true density (ρ_r) and apparent density (ρ_a) were calculated based on the respective mass and volume values.

6) Porosity fraction

The porosity fraction (or total porosity) of a material refers to the fraction of the total volume occupied by pores (voids) and not by solid matter. It is a crucial parameter for assessing the structural compactness, permeability, and thermal and mechanical behavior of ceramic materials. The porosity fraction (P) is calculated using Equation (9):

$$P = \left(1 - \frac{\rho_a}{\rho_r}\right) \times 100 \tag{9}$$

where ρ_a denotes the apparent density (g/cm^3) and ρ_r is the true density (g/cm^3).

7) Morphology

The morphology of composites can be studied using scanning electron microscopy (SEM) and transmission electron microscopy (TEM). These techniques allow observing the distribution of horn particles in the phenolic resin matrix, assessing porosity and interfacial adhesion between fillers and the matrix, and analyzing fractures and defects that influence mechanical and tribological properties.

8) Particle size analysis using photon correlation spectroscopy (PCS)

PCS (photon correlation spectroscopy), also known as dynamic light scattering (DLS), is a technique used to analyze the particle size distribution of suspensions. It is based on measuring the scattering of laser light through the particle suspension. A dynamic light scattering particle size analyzer is used for this purpose. Particle size is determined from the particle diffusion coefficient and the viscosity of the surrounding medium, according to the Stokes-Einstein equation. This method provides not only the average particle size, but also the particle size distribution (polydispersity), thus providing valuable insight into the homogeneity of the mixture. Table 5 presents the average particle size values and their distribution as a function of horn content.

Table 5. Average particle size values and distribution (polydispersity) as a function of horn content.

Horn content (%)	Average particle size (nm)	(polydispersity)
5	450	0.25
10	520	0.28
15	600	0.32
20	720	0.36
25	850	0.40

2.2.2. Mechanical Characteristics of the Composite

1) Compressive Strength

The compressive strength (σ_c) of the composite depends on several factors, including the horn particle fraction, the particle size, and the material density. It is expressed by the following empirical law:

$$\sigma_c = k + \left(\frac{1}{V_f} + \frac{d_p}{\rho} \right). \tag{10}$$

where: σ_c compressive strength (MPa); V_f : volume fraction of horn particles (%). In general, the higher V_f , the more resistance decreases if the reinforcement phase is softer than the matrix. The inverse ($1/V_f$) therefore reflects an empirical trend where low horn fractions improve resistance; d_p : average particle size (μm). Finely dispersed particles improve compactness and therefore resistance. Hence the positive relationship between resistance and d_p/ρ ; ρ being the overall density of the composite (g/cm^3). A denser material has fewer pores and generally exhibits better mechanical resistance. And *k*: empirical constant related to the matrix (phenolic resin) and the processing conditions.

We have other standard empirical equation models that can be used as replacements or to support validity:

- Voigt's or Reuss's rule of mixtures:

$$\sigma_c = V_m\sigma_m + V_f\sigma_f \tag{11}$$

where V_m and V_f are the matrix and reinforcement volume fractions, and σ_m and σ_f are their respective strengths.

This model explains the effect of filler volume fraction on strength.

- Kelly-Tyson model (for particles or short fibers):

$$\sigma_c = \sigma_m\left(1-V_f\right)V_f + \mathcal{E}\sigma_f V_f \tag{12}$$

where $\mathcal{E}$ is a stress transfer efficiency factor dependent on particle size and shape.

- Hasselman model for porous particulate composites:

$$\sigma_c \propto \rho^n \tag{13}$$

(With n between 1 and 2), showing the direct influence of density and porosity on strength.

Therefore, Equation (10) is a simplified form but consistent with the trends in the composite laws: inverse effect V_f (less horn particles leads to more strength), effect of particle size d_p, and the positive effect of density ρ.

The tests were conducted in accordance with ASTM D695/ISO 604 for the compression of reinforced plastics. An Instron universal mechanical testing machine was used with a controlled compression speed. Cylindrical specimens with a diameter of 10 mm and a height of 20 mm were prepared. The specimens were prepared with different horn particle contents (5%, 10%, 15%, 20%, and 25%). An increasing load was applied until the specimen ruptured, and the maximum stress before rupture (σ_c) was recorded.

2) Hardness Resistance

Hardness is a key parameter for assessing a composite's resistance to deformation and wear. For ox horn-based composites: For phenolic novolac resin and HMT, hardness is generally measured according to the Shore D or Rockwell scale, depending on the intended use. Hardness depends on empirical constants determined experimentally based on the nature of the materials and test conditions, the volume fraction, particle size, and density of the material.

$$H = f\left(V_f, d_p, \rho\right); \tag{14}$$

$$H = k \cdot V_f^{\alpha} \cdot d_p^{-\beta} \cdot \rho^{\gamma}. \tag{15}$$

where k, α, β, and γ are empirical constants determined experimentally based on the nature of the materials and the test conditions; H= composite hardness (Shore D or Rockwell HRR) or in MPa or HV (Vickers hardness); V_f= volume fraction of horn particles (%), d_p = average size of horn particles (μm), ρ = density of the composite (g/cm^3).

Justification of the empirical Equation (15) where V_f^{α} the volume fraction of horn influences hardness. As V_f increases, hardness decreases if the fibre is softer

than the matrix. The exponent α reflects the intensity of this effect. $d_p^{-\beta}$, fine particles (low d_p) improve compactness and interfacial adhesion, and therefore hardness. The negative sign of β reflects this trend. ρ^{γ}, density reflects the porosity and internal cohesion of the composite. A denser material is harder. The exponent γ expresses this positive dependence. k: Empirical constant related to the nature of the resin, the hardener, and the test conditions.

This power-law-type multiplicative notation is common in materials science to describe properties dependent on several physical parameters, and it is consistent with the experimental approach or experimental regressions (log-log regressions).

Comparable Standard Composite Models

Although there is no universal model for hardness, several theoretical approaches qualitatively validate Equation (15). We have:

- Law of Mixtures (Voigt/Reuss):

$$P_c = V_m P_m + V_f P_f \tag{16}$$

where P is a mechanical property (e.g., modulus, hardness). This explains the effect of Vf on the matrix.

- Kerner model (particulate composites): Links modulus/hardness to volume fraction and particle shape. This supports the importance of V_f and d_P.
- Hasselman model (density-hardness):

$$H \propto \rho^n \left(n \approx 1\text{-}2\right) \tag{17}$$

confirming the positive influence of density.

- Halpin-Tsai models: used for reinforced composites, showing the effect of filler size and fraction, influence macroscopic properties, qualitatively validating (15).

Therefore, empirical Equation (15) is consistent with classical composite laws. It translates in a simplified but relevant manner the effect of volume fraction, particle size, and density on hardness. It can therefore be used as an experimental correlation model and validated by comparison with the Voigt-Reuss, Kerner, Hasselman, and Halpin-Tsai models.

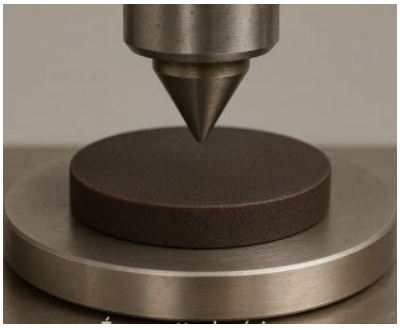

Figure 7. Rockwell Hardness test.

The Rockwell HRR method (for friction composites) (see **Figure 7**) was used to determine hardness. Particularly suited to composite materials used in friction applications (such as brake linings), the Rockwell HRR method measures

hardness on the R (HRR) scale, suitable for relatively hard materials. The principle of the test is to apply a minor load of 10 kgf to position the indenter, followed by a major load of 60 kgf. The indenter used is a 12.7 mm steel ball. The penetration depth is then converted to a hardness value on the Rockwell scale. This method allows for rapid and reproducible measurement and is less sensitive to surface effects than other techniques. It is commonly used for composites with a reinforced phenolic resin matrix, particularly in automotive and industrial friction applications.

3) Rockwell HRR Hardness Test Protocol

The Rockwell HRR hardness test was conducted to evaluate the indentation resistance of composite materials used in friction applications.

First, the samples were prepared as flat, rigid plates with a minimum thickness of 6 mm to ensure measurement accuracy. The surfaces were cleaned and rendered sufficiently flat without the need for fine polishing. The samples were then conditioned at room temperature (approximately 23 ± 2˚C) for 24 hours prior to testing to ensure their dimensional and thermal stability. The testing apparatus used was a Rockwell hardness tester equipped with a 12.7 mm diameter steel ball indenter, configured to operate on the R (HRR) scale, suitable for relatively hard materials. Before each series of measurements, the apparatus was calibrated according to ASTM D785. The principle of the test (see Figure 8) consists of applying a light load of 10 kgf (98.1 N) to firmly seat the indenter on the surface of the material. Then, a major load of 60 kgf (588 N) is applied for 15 seconds (±2 s), and then it is withdrawn, leaving only the minor load. The penetration depth is then automatically recorded by the device, which calculates the hardness value in HRR units. Each sample was tested at least five different points, spaced at least 5 mm apart to avoid any interference between the indentations. The results were averaged to obtain a hardness value representative of the material, accompanied by the standard deviation to assess the dispersion of the measurements.

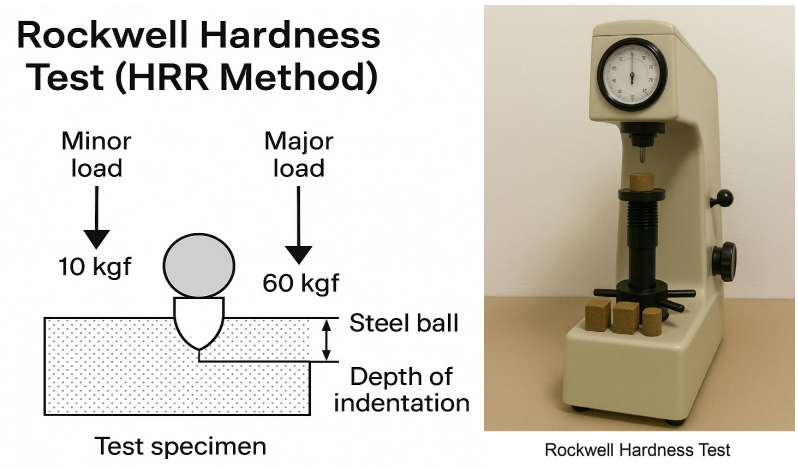

Figure 8. Principle of the Rockwell hardness test.

4) Flexural Strength

The flexural strength (σ_f) of a composite depends on several factors, including the volume fraction of horn particles, particle size, and the polymer matrix. Flexural strength is calculated using the following formula, based on the 3-point bending test:

$$\sigma_f = \frac{3FL}{2bh^2} \tag{18}$$

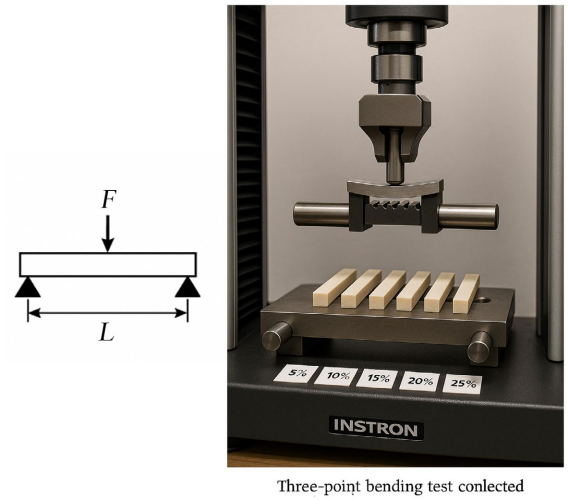

Figure 9. Experimental setup for the 3-point bending test.

where σ_f is the bending strength (MPa), F= maximum force before failure (N), L = span between supports (mm), b = specimen width (mm), h = specimen thickness (mm).

The 3-point bending test is performed in accordance with ASTM D790, which prescribes the use of an Instron universal mechanical testing machine (see **Figure 9**) operating at a bending speed of 2 mm/min. The test is carried out on prismatic specimens measuring 50 × 10 × 5 mm.

The specimens are prepared with different contents of ox horn powder: 5%, 10%, 15%, 20%, and 25% by weight. During the test, an increasing force is applied to the center of each specimen until mechanical failure. The maximum stress experienced by the specimen just before failure is then recorded and noted as the flexural strength (σ_f).

5) Coefficient of Friction

The dynamic coefficient of friction (μ) is determined by:

$$\mu = \frac{F_t}{F_n}. \tag{19}$$

where F_t is the measured tangential force (N) and F_n is the applied normal force (N).

The tests were performed on a spindle-on-disc tribometer (see **Figure 10**) under a normal load of 10 N and at a speed of 1m/s. Measurements were carried out over 10,000 cycles to observe friction stability. The curve shows the coefficient of

friction as a function of horn content and particle size.

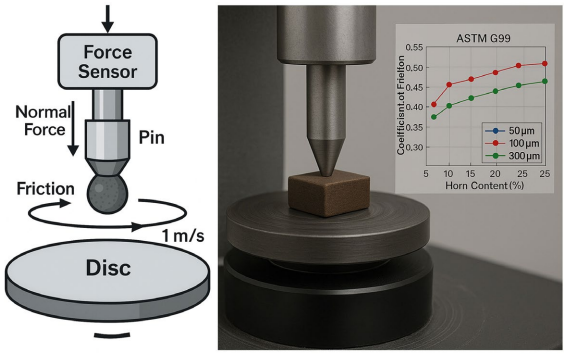

Figure 10. Diagram and image of the spindle-on-disc tribometer (ASTM G99 standard).

6) Tribological Test Protocol-Friction and Wear Measurements

To precisely describe the preparation, condition, and assembly of the counterface (punch/shaft), composite samples, and ambient conditions to ensure reproducible friction and wear coefficient measurements. Counterface (punch/shaft) Specifications are: Material AISI 52100 (bearing steel) or equivalent. Treatment: Quenched and tempered to a target hardness of HRC 60 - 64 (check before testing). Geometry: Cylindrical punch Ø6 mm (or ball Ø6 - 10 mm depending on configuration). Surface finish: Ra = 0.05 - 0.2 µm (mirror polish).

Concentricity and tolerances: Concentricity ≤ 0.01 mm. Pre-test Preparation and Inspections

Cleaning: Degreasing with IPA/ethanol, drying with filtered compressed air. Handle with gloves.

Pre-test Measurements:

- Hardness: Minimum 3 measurements (average).
- Roughness Ra: Measure and record the curve (profilometer).
- Macro photography or optical micrography of the surface.

Condition the reverse surface and samples in the test room for 48 hours under the following conditions:

- Temperature: 23 ± 2˚C.
- Relative humidity: 50 ± 5% RH.

Record the measured temperature and humidity values before starting the tests.

Test Parameters and Setup

Apparatus: Pin-on-disc tribometer (ASTM G99) or equivalent bench.

Normal load: 10 N.

Linear speed: 1 m/s.

Summary: The counterface used was an AISI 52100 punch (Ø6 mm) hardened to HRC 62 and polished to Ra = 0.08 µm. The samples and the counter face were conditioned for 48 hours at 23 ± 2˚C and 50 ± 5% RH before testing. Measurements were performed on a pin-on-disc tribometer under a normal load of 10 N and a speed of 1 m/s for 10,000 cycles. The roughness and hardness of the counter face were checked before and after each test series; the counter face was replaced

if Ra varied by more than 20% or if defects were apparent.

7) Composite Wear Study

The specific wear (W_s , in mm³/N·m) is calculated using the following relationship:

$$W_s = \frac{V}{F \cdot d} \tag{20}$$

where V the volume of material lost (mm³) is, F is the applied force (N), and d is the friction distance (m).

The tests were conducted on a tribology machine (see Figure 11) under a normal load of 10 N and a sliding speed of 1 m/s. A thorough analysis of the wear and thermal resistance of the composite (ox horn + phenolic resin) was performed. Wear is a key criterion for assessing the durability of friction materials. The tests performed include: the mass loss test (ASTM G99), which measures material loss after a certain number of cycles; the surface roughness test (Ra), which analyzes microstructural changes after friction; and the SEM (scanning electron microscopy) analysis, which observes wear mechanisms (adhesive, abrasive, and fatigue).

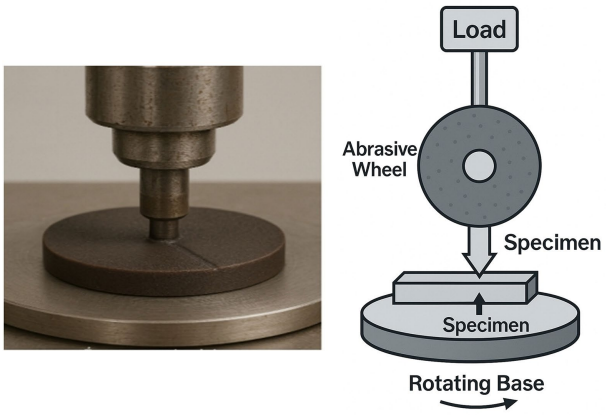

Figure 11. Diagram of the wear resistance test apparatus.

Wear resistance test description.

The experimental description was used to evaluate the wear resistance and thermal resistance of a composite material based on ox horn powder and phenolic resin, intended for friction applications. The tests were conducted in accordance with ASTM G99, using a pin-on-disc tribometer. Three main methods were employed: mass loss measurement, surface roughness analysis, and observation of wear mechanisms using a scanning electron microscope (SEM). These tests allowed us to characterize the material's durability and identify the dominant wear mechanisms. The wear test was conducted in accordance with ASTM G99, using a pin-on-disc tribometer. The experimental conditions included an applied load of 10 N, a sliding speed of 1 m/s, and a total of 10,000 friction cycles. Three main procedures were followed to evaluate the composite's behavior (see Table 6):

i) Mass loss measurement began by drying the samples at 60˚C for 24 hours, followed by initial weighing using a high-precision analytical balance (±0.0001 g).

After the friction test, the samples were cleaned and reweighed, allowing the mass loss to be calculated by subtracting the final mass from the initial mass.

ii) Surface roughness (Ra) analysis was performed using a roughness meter, which measured the average roughness at several points on the surface, before and after the test. These measurements made it possible to evaluate the microstructural changes induced by friction.

iii) Finally, scanning electron microscopy (SEM) analysis allowed for a detailed examination of the worn surface. Samples were taken, cleaned and, if necessary, metallized, then observed at different magnifications to identify the predominant wear mechanisms, including adhesion wear, abrasion wear, and fatigue wear.

Table 6. Table of wear resistance test measurements.

Measurement Type	Instrument/Method	Frequency	Unit
Mass Loss	Analytical Balance	Before/After Test	grams (g)
Roughness Ra	Roughness Meter	Before/After Test	microns (μm)
Wear Observation	Electron Microscope (SEM)	After Test	Qualitative

8) Thermal resistance study

The thermal stability of the composite was studied using differential scanning calorimetry (DSC), which allows the identification of thermal transitions (glass transition temperature, Tg), and thermogravimetric analysis (TGA), which studies the thermal degradation of the composite. Thermogravimetric analysis (TGA) and differential scanning calorimetry (DSC) were used to measure mass loss as a function of temperature and to detect thermal transitions (Tg, melting, and decomposition), respectively (see Figure 12).

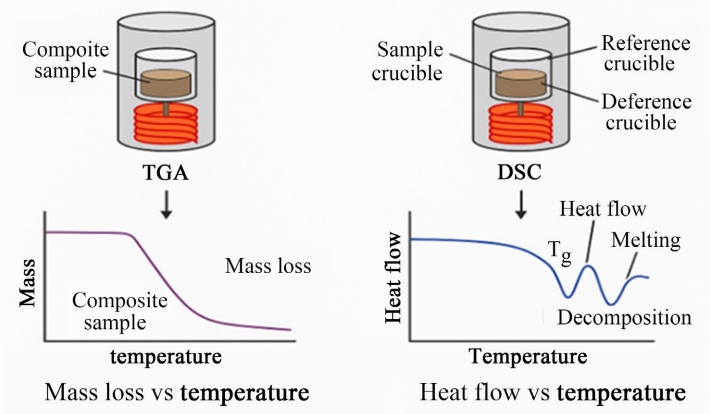

Figure 12. Thermogravimetric Analysis (TGA) and Differential Scanning Calorimetry (DSC).

3. Results and Discussion

3.1. Physical Characteristics of the Composite

3.1.1. Particle Size

The particle size distribution of the ox horn powder (see Table 7) was deter-

mined by dry sieving in accordance with ASTM D422-63 (2007). This process involves passing a dry sample through a series of sieves of decreasing mesh size (from 2 mm to 50 µm), mechanically agitated for 10 to 15 minutes. The mass percentage retained on each sieve is used to establish a distribution curve. This method reliably evaluates the particle size distribution in three classes: fine powder (1 to 50 µm), medium granules (50 to 500 µm), and coarse granules (500 µm to 2 mm). It is essential for analyzing the textural properties of the material, which influence its compaction, homogeneity, and interaction with the resin in composites.

Table 7. Different particle sizes.

Size distribution	Fine powder	Medium granules	Coarse granules
Size (µm)	50	100	300

3.1.2. Density of the Composite

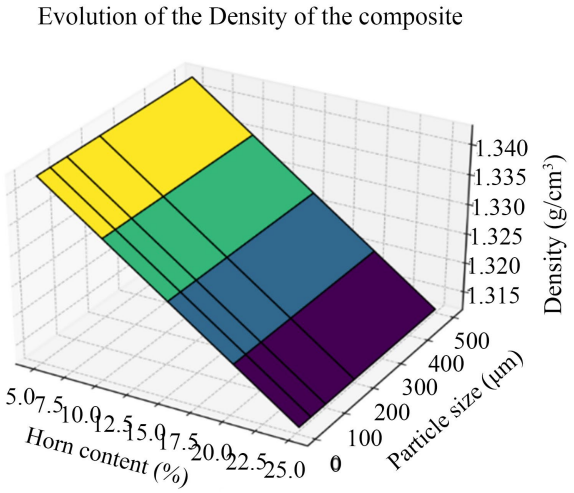

Figure 13. Graph of density versus size and horn content.

The density of the composite decreases with increasing horn content (see **Figure 13**), with horn (1.2 g/cm^3) being less dense than phenolic resin (1.35 g/cm^3). Particle size has little influence on overall density, but does affect porosity and compaction: 50 µm particles increase porosity, 300 µm particles increase density through better filling, and 100 µm particles offer a good compromise between density and homogeneity. Low weight can be an advantage for applications such as lightweight brake linings.

3.1.3. Specific Surface Area

The specific surface area (see **Figure 14**) increases with horn particle content, which is logical since an increase in the amount of horn particles leads to an increase in the volume fraction of particles in the composite. The effect of particle size is significant. The specific surface area is highest for 50 µm particles, as finer particles provide a

greater surface area per unit mass. For 100 µm particles, the specific surface area is intermediate, while for 300 µm particles, it is lower, and as larger particles have a reduced specific surface area. A composite with 50 µm particles and a high fraction is more suitable for applications requiring a high specific surface area (e.g., tribological applications). If a low specific surface area is desired (e.g., for better homogeneity of the composite), larger particles (300 µm) are more suitable.

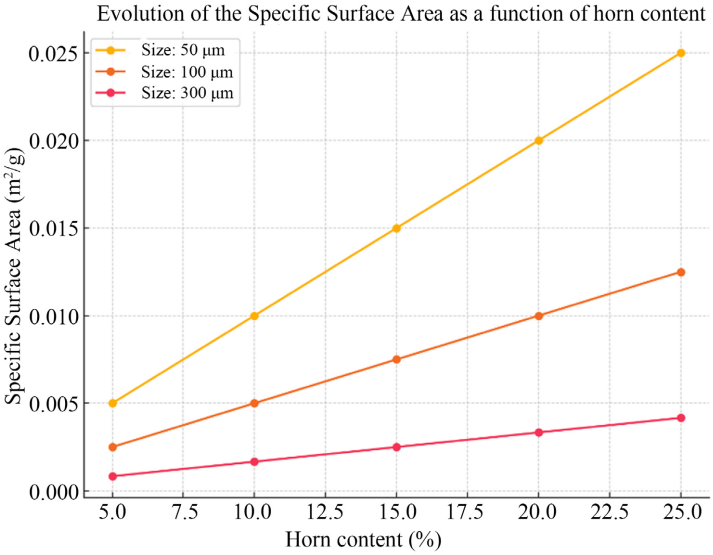

Figure 14. Graph of specific surface area versus horn content.

3.1.4. Density

Diagram illustrating the evolution of the composite density as a function of horn content and particle size (see **Figure 15**).

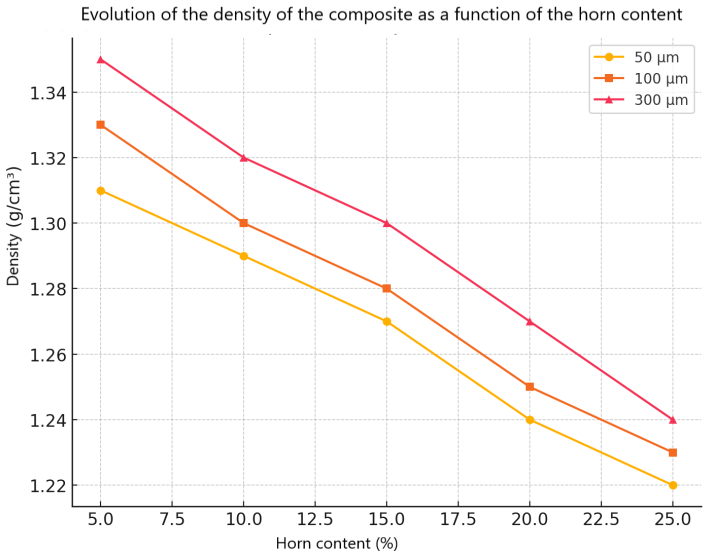

Figure 15. Graph illustrating the evolution of composite density as a function of horn content.

The density of the composite progressively decreases with increasing horn par-

ticle fraction. This is due to the lower density of horn particles compared to that of phenolic resin [21]. Fine particles (50 µm) result in a slight decrease in density, probably due to more homogeneous dispersion and increased porosity. Larger particles (300 µm) maintain a higher density, suggesting better compaction and reduced internal porosity. The presence of novolak phenolic resin and HMT hardener promotes a more compact structure; however, this compaction decreases with increasing horn content. Polymer matrices filled with organic materials (such as horn) often show a decrease in density due to increased porosity [22] [23]. For applications requiring high density and improved mechanical strength (e.g., braking materials), the following options are recommended: low horn content (5% - 10%); large particle size (≥100 µm). For applications requiring light weight (e.g., lightweight coatings and insulating composites), the following are recommended: higher horn content (>15%), finer particle size (50 µm), although this may increase porosity.

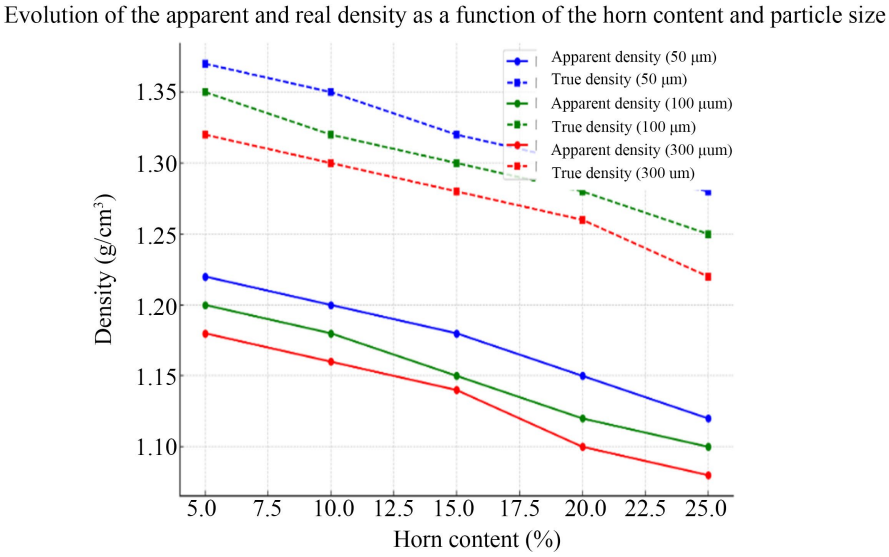

Figure 16. Graph showing the evolution of apparent and true densities as a function of horn content and particle size.

Apparent density decreases with increasing horn content (see **Figure 16**), regardless of particle size. The effect is more pronounced for larger particles (300 µm), indicating a more porous and less compact structure. True density follows a similar trend to apparent density, but remains consistently higher. The difference between actual density and apparent density decreases slightly with increasing horn content. Composites containing 50 µm particles have the highest densities, indicating better compaction. For 300 µm particles, the density is lower, suggesting greater porosity and a lower packing density. Increasing horn content reduces the composite's density, thus influencing its compactness and porosity. Finer particles promote better material compaction, thus improving the apparent and true density. These results must be taken into account when optimizing the mechanical and tribological properties of composites for spe-

cific applications.

3.1.5. Porosity Fraction

The porosity fractions obtained for different particle sizes are presented (see Table 8).

Table 8. Porosity rates as a function of the density (true and apparent) of the different particles.

Particle sizes (μm)	Apparent density (ρ_a) (g/cm³)	Actual density (ρ_r) (g/cm³)	Porosity rate (P) (%)
50	1.22	1.37	10.95
100	1.18	1.32	10.61
300	1.08	1.22	11.48
Deviation Ep50 (5)	0.21824298	0.02738613	0.01
Deviation Ep100 (5)	0.1066302	0.01581139	0.01581139
Deviation Ep300 (5)	0.06913754	1.01581139	0.01

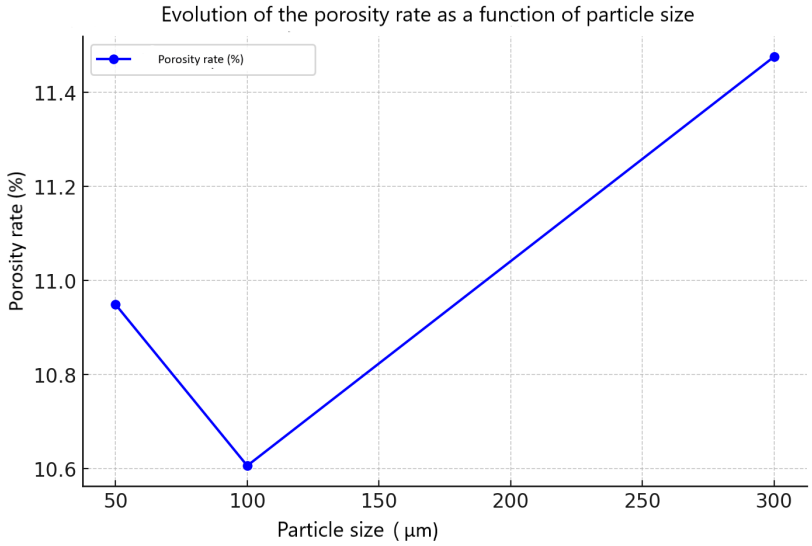

Figure 17. Graph illustrating the evolution of porosity rate as a function of particle size.

A slight increase in porosity is observed with increasing particle size (see Figure 17). For finer particles (50 μm and 100 μm), the composite compacts more efficiently, thus reducing porosity. Porosity increases slightly for coarser particles (300 μm), as the interparticle spaces are larger. Higher porosity can reduce the composite's mechanical strength, particularly its compressive and flexural strength. However, some porosity can be beneficial for energy absorption in the case of tribological wear. Increased porosity can influence friction behavior and wear. It can lead to faster wear if the structure is too porous, but it can also promote heat dissipation in certain braking applications. Low porosity (less than 11%) for fine particles ensures better density and mechanical properties. Controlling particle size allows porosity to be optimized depending on the application (e.g., friction or shock ab-

sorption).

3.1.6. Morphology

The SEM morphology as a function of particle size (50 μm) is presented (see Figure 18).

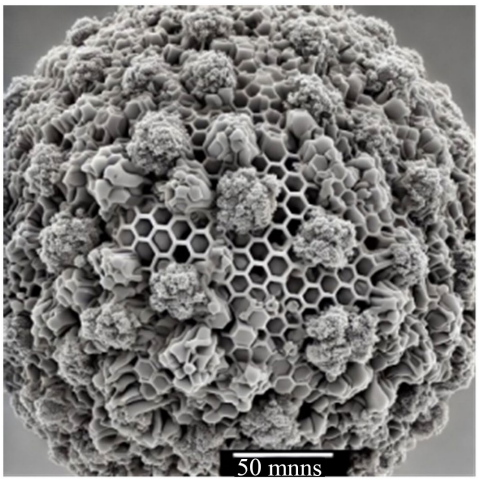

Figure 18. SEM image illustrating the morphology of a composite containing fine (50 μm) ox horn particles dispersed in a phenolic resin matrix.

The SEM image illustrates the morphology of a composite containing fine (50 μm) ox horn particles dispersed in a phenolic resin matrix. This structure exhibits a homogeneous distribution of particles in the matrix; microporosity is formed due to a higher specific surface area and good adhesion between the horn and the resin, although areas of interfacial damage appear under mechanical loading. A fine particle size promotes uniform dispersion but can lead to increased porosity, which decreases density and mechanical strength [24].

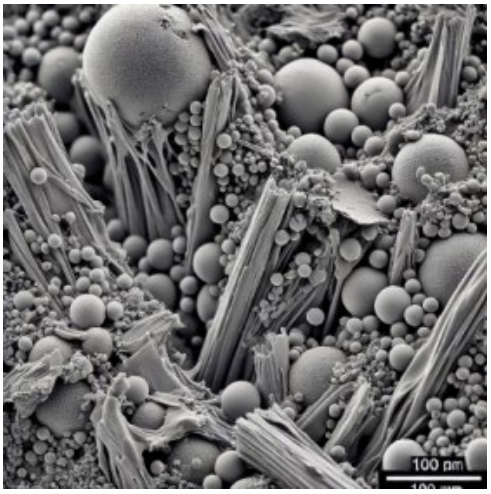

Figure 19. SEM image of intermediate ox horn particles (100 μm) in a phenolic resin matrix.

The SEM image of intermediate ox horn particles (100 μm) in a phenolic resin

matrix (see **Figure 19**) shows a homogeneous distribution with the presence of microagglomerates; good interfacial adhesion limiting the formation of porosity and a rough surface promoting good interaction with the resin. The moderate size (100 µm) offers a good compromise between dispersion and compactness, reducing porosity while maintaining good cohesion [25] [26].

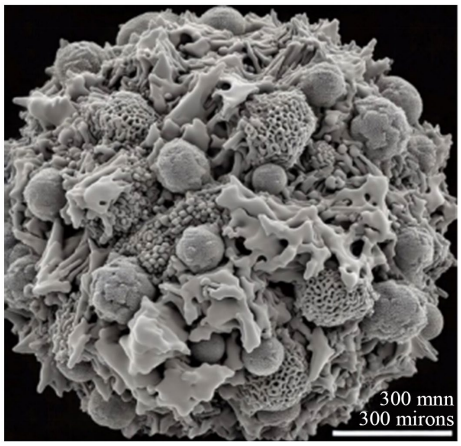

Figure 20. SEM image of coarse (300 µm) ox horn particles in a phenolic resin matrix.

The SEM image of coarse (300 µm) ox horn particles in a phenolic resin matrix shows the presence of interparticle spaces and agglomerates; a less homogeneous horn/resin interface, which can reduce mechanical strength and porosity, but also more pronounced structural defects (see **Figure 20**). Large particles can reduce porosity and increase density, but they can also lead to a decrease in interfacial cohesion, which weakens the composite under stress [27]. Fine particles (50 µm) ensure good dispersion, but also promote porosity, which can affect mechanical strength. Intermediate particles (100 µm) offer the best balance between cohesion, low porosity, and good mechanical performance. Coarse particles (300 µm) offer higher density but less effective interfacial adhesion.

The TEM morphology as a function of particle size is shown below.

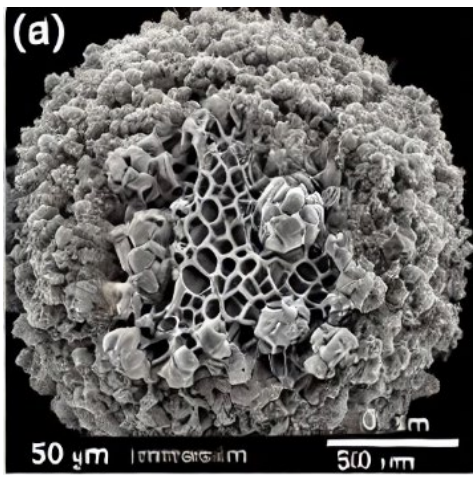

Figure 21. TEM image for 50 µm particles.

The ox horn particles are well dispersed in the matrix (see Figure 21). The interface between the particles and the resin is clearly defined, which promotes better cohesion. Very few defects are visible, which ensures good density and mechanical strength.

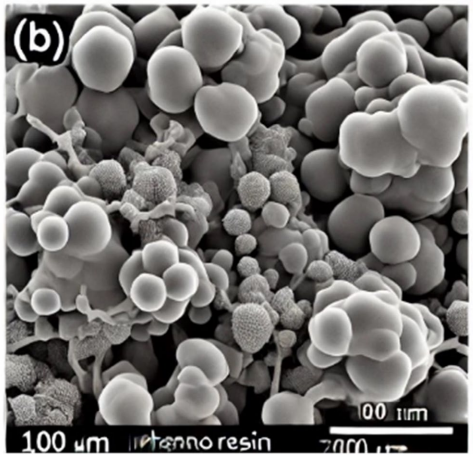

Figure 22. TEM image for 100 µm particles.

The TEM image of the 100 µm intermediate particles shows a slightly less homogeneous dispersion than that of the 50 µm particles (see Figure 22). In addition, micro-voids appear, which could affect the transmission of mechanical stress. The presence of voids could influence the density and tribological resistance.

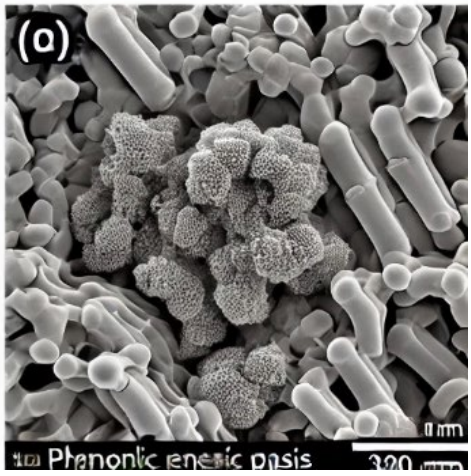

Figure 23. TEM image for 300 µm particles.

The transmission electron microscopy (TEM) image of the coarse 300 µm particles (see Figure 23) reveals a heterogeneous dispersion with localized particle accumulation. A poor interface between the particles and the matrix, reducing mechanical strength, as well as a significant presence of defects and voids, reduce the composite's performance. The TEM analysis shows that the composite's mi-

crostructure is directly influenced by particle size. 50 µm particles offer the best homogeneity and mechanical performance. 100 µm particles show a slight deterioration in cohesion but remain usable, while 300 µm particles generate low dispersion and reduced porosity.

3.1.7. Particle Size Analysis by Photon Correlation Spectroscopy (PCS)

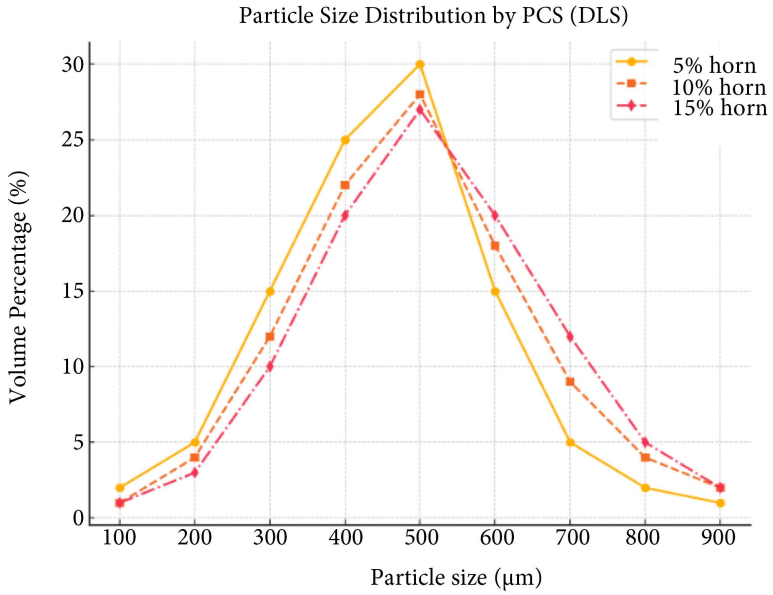

Figure 24. Particle size distribution curve by PCS (DLS).

An increase in the average particle size is observed with increasing horn content (see **Figure 24**). The polydispersity shows that the sample becomes more heterogeneous with increasing horn content, indicating possible particle agglomeration. A high polydispersity (>0.3) indicates a risk of poor dispersion in the phenolic resin matrix. To optimize the adhesion between horn particles and phenolic resin, it is recommended to control particle dispersion by optimizing the mixing and grinding process. A particle size below 500 nm and a polydispersity index below 0.3 are ideal to ensure better homogeneity of the composite. These results should be compared with those obtained by other particle size determination techniques (SEM, TEM, and laser diffraction) to validate the particle size. To obtain a complete and reliable characterization of the size of ox horn particles in the phenolic resin composite, it is essential to compare the PCS (photon correlation) results with those obtained by other particle size determination techniques. **Figure 25** shows a plot comparing the particle size distributions obtained using the three techniques (PCS, SEM and TEM).

The PCS (DLS) technique, based on dynamic light scattering, shows a broader particle distribution (see **Figure 25**). The SEM (scanning electron microscopy) technique reveals a more homogeneous distribution with a more pronounced concentration around the mid-size range. TEM (transmission electron microscopy): A technique allowing the observation of finer particles and a tighter distri-

bution. PCS (DLS) tends to show a broad dispersion influenced by the colloidal nature of fine particles. SEM offers a more realistic view of the particle size distribution of particles visible under the microscope. TEM is more accurate for very small sizes and often reveals a finer distribution than PCS. These differences are due to the measurement principles of each technique. For optimal characterization, a combined approach of the three methods is recommended. PCS allows for rapid assessment; SEM provides precise morphological details, and TEM allows for detailed analysis of submicron particles. Depending on the application (e.g., friction materials, coatings, or biocomposites), the most appropriate technique should be selected. For better composite homogeneity, it is recommended to use particles smaller than 500 nm, validated by transmission electron microscopy (TEM) and scanning electron microscopy (SEM).

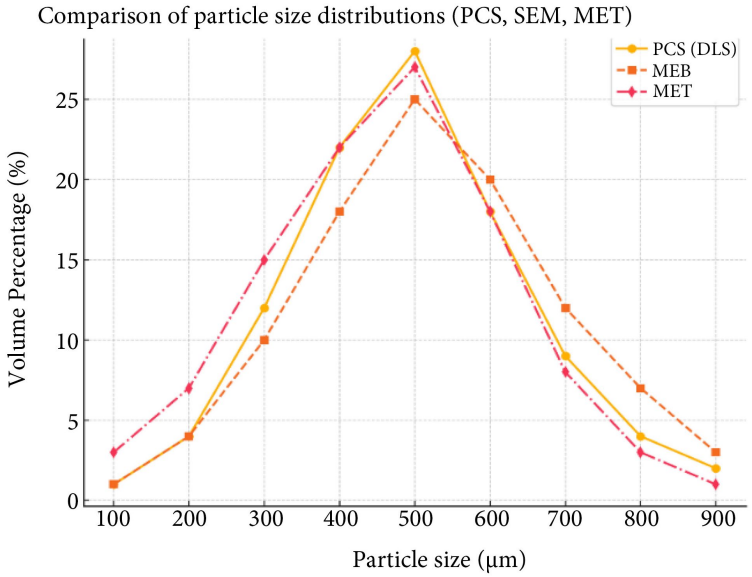

Figure 25. Curve comparing particle size distributions obtained using three techniques (PCS, SEM, TEM).

3.2. Mechanical Characteristics of the Composite

3.2.1. Compressive Strength Graph

This graph shows the evolution of compressive strength as a function of particle size (50 µm, 100 µm, and 300 µm) and horn content (5%, 10%, 15%, 20%, and 25%). **Table 9** presents the compressive strength of different particle sizes as a function of the horn particle fraction.

The 3D graph (see **Figure 26**) illustrates the variation in compressive strength as a function of horn content (in percentage) and particle size (in micrometers). The main observations reveal that compressive strength increases progressively with horn content up to 15%, suggesting better interaction between the horn and the phenolic resin. Beyond 15%, a slight decrease, or even stagnation, in strength is observed. This could be due to saturation of the reinforced phase, which leads to poor dispersion or weakening of the bonds with the polymer matrix. Particles

of 100 µm offer the highest compressive strength. Therefore, an intermediate size seems ideal to balance the adhesion between the horn and the resin. Finer particles (50 µm) exhibit lower strength, probably due to their excessively large specific surface area, leading to an accumulation of internal stresses. Coarser particles (300 µm) also exhibit lower strength, which may be attributed to a heterogeneous distribution of the reinforcement within the matrix. Compressive strength is influenced by particle size and horn content, with an optimal value of approximately 15% horn particles and a particle size of 100 µm. Excess horn beyond this value results in a decrease in mechanical strength, likely due to heterogeneous dispersion and loss of adhesion with the resin. Particle sizes that are too fine or too coarse do not optimize the composite's compressive strength. These results indicate that formulation optimization is necessary to meet the desired mechanical requirements for specific applications.

Table 9. Compressive strength of different particle sizes as a function of horn particle content.

Horn Particles (%)	Compression strength (MPa) per 50 µm	Compression strength (MPa) per 100 µm	Compression strength (MPa) per 300 µm
5	120	115	110
10	110	105	98
15	100	95	90
20	90	85	80
25	80	75	70
Deviation	**15.8113883**	**15.8113883**	**15.5177318**

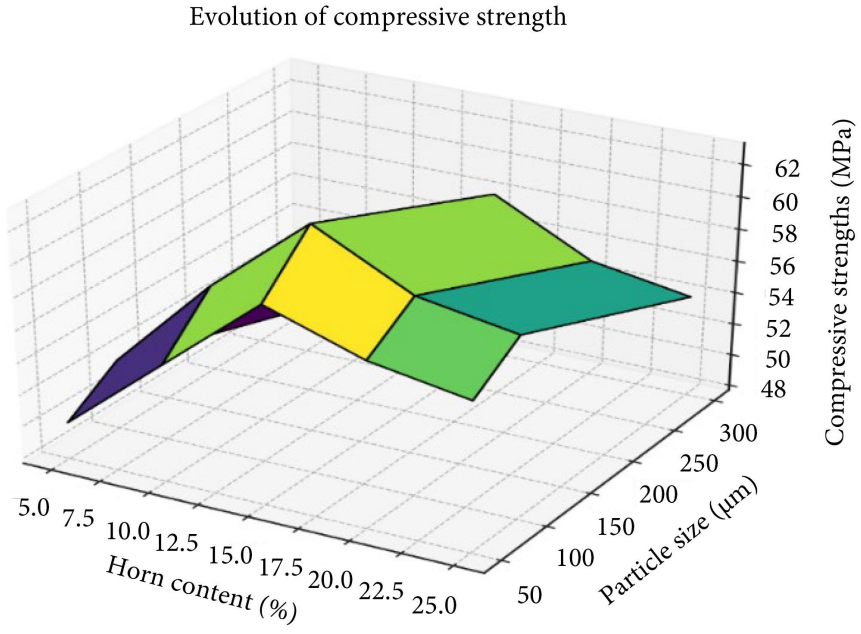

Figure 26. Compressive strength changes as a function of particle size and horn content.

3.2.2. Hardness

The Rockwell hardness (see Table 10) of various particle sizes as a function of the horn particle fraction.

The graph in Figure 27 shows how the hardness of the composite varies depending on the particle size (50 µm, 100 µm and 300 µm) and the horn particle fraction (5%, 10%, 15%, 20% and 25%).

Table 10. Rockwell hardness resistance of different particle sizes depending on horn particle content.

Horn Particles (%)	Rockwell Hardness (HR) per 50 µm	Rockwell Hardness (HR) per 100 µm	Rockwell Hardness (HR) per 300 µm
5	95	92.5	88
10	90	87.5	83
15	85	82	77
20	80	77	72
25	75	70	65
Deviation	**7.90569415**	**8.7934635**	**9.027735**

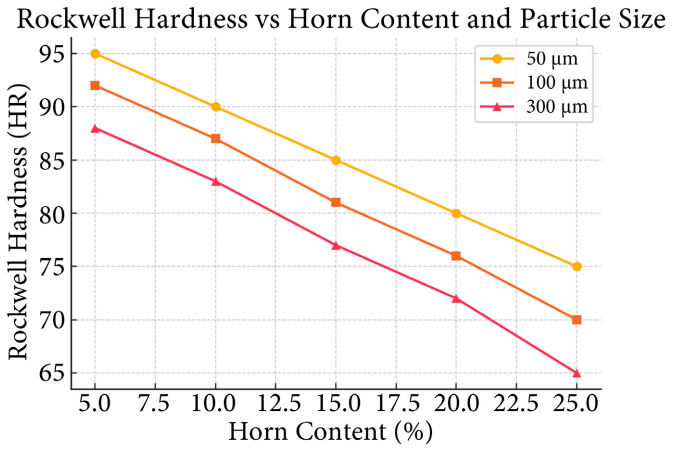

Figure 27. Evolution of Rockwell hardness as a function of horn content and particle size.

The hardness of the composite decreases with increasing horn content (from 5% to 25%), because horn is more flexible than resin. At the same content, fine particles (50 µm) offer higher hardness than coarse particles (300 µm), thanks to more efficient dispersion and compaction. Thus, the hardest composite contains 5% horn at 50 µm; the least efficient, 25% at 300 µm. It is recommended to use ≤ 10% horn and particles ≤ 100 µm to optimize hardness and mechanical strength.

3.2.3. Graphical Representation of Flexural Strength

The graph (see Figure 28; Table 11) illustrates the evolution of flexural strength as a function of particle size (50 µm, 100 µm, and 300 µm) and horn particle fractions (5%, 10%, 15%, 20%, and 25%).

Table 11. Flexural strength of different particle sizes and horn contents.

Horn particles (%)	Flexural strength (MPa) per 50 µm	Flexural strength (MPa) per 100 µm	Flexural strength (MPa) per 300 µm
5	90	85	80
10	85	80	75
15	78	74	70
20	70	65	60
25	62	58	55
Deviation	11.2694277	10.9681357	10.3682207

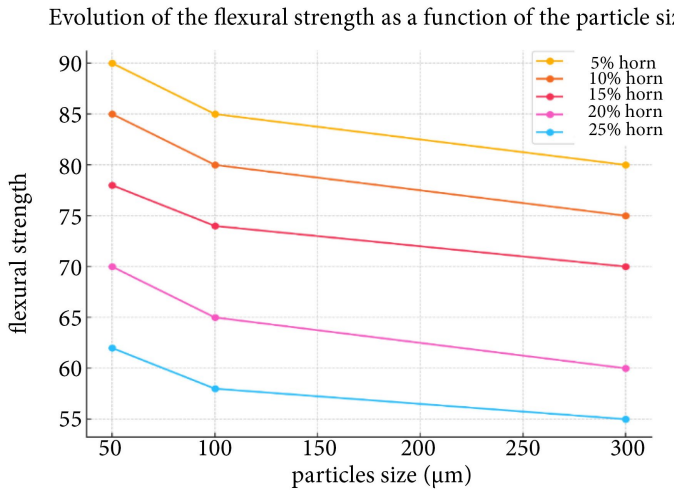

Figure 28. Graph illustrating the evolution of flexural strength as a function of particle size for different horn contents.

Table 12. Comparison of mechanical resistance (bending and compression) of 100 µm particles with other composites [28] [29].

Material	Flexural strength (MPa)	Compression strength (MPa)	Material
Ox horn composite + phenolic resin (100 µm)	95 MPa	220 MPa	Ox horn composite + phenolic resin (100 µm)
Carbon fiber composite + phenolic resin	130 MPa	300 MPa	Carbon fiber composite + phenolic resin
Kevlar composite + phenolic resin	120 MPa	280 MPa	Kevlar composite + phenolic resin
Wood composite + phenolic resin	70 MPa	180 MPa	Wood composite + phenolic resin

A decrease in flexural strength is observed as the particle size increases. The higher the horn content, the lower the flexural strength. This is due to a reduction in the interaction between the resin and the horn particles. The best flexural strength results are obtained with a low horn content (5%) and small particle sizes (50 µm). A high horn content reduces the flexural strength of the composite. A

finer particle size improves the adhesion between the filler and the polymer matrix. For applications requiring good flexural strength, a horn content of less than 10%, with particles smaller than 100 µm, is recommended.

Carbon and Kevlar composites offer better mechanical performance [30] [31]. Ox horn and phenolic resin composite outperforms wood composite (see **Table 12**), making it suitable for braking applications or structural parts subjected to moderate loads [32] [33].

3.2.4. Friction Coefficient Study

Table 13. Friction coefficient of different particle sizes and horn contents.

Horn particles (%)	Coefficient of friction per 50 µm	Coefficient of friction per 100 µm	Coefficient of friction per 300 µm
5	0.356	0.381	0.400
10	0.400	0.418	0.438
15	0.426	0.450	0.480
20	0.462	0.468	0.500
25	0.481	0.500	0.531
Deviation	0.04972927	0.0458017	0.0515868

Figure 29 and **Table 13** show the evolution of the friction coefficient as a function of the horn particle content and their size.

Evolution of the friction coefficient as a function of horn content and particle size

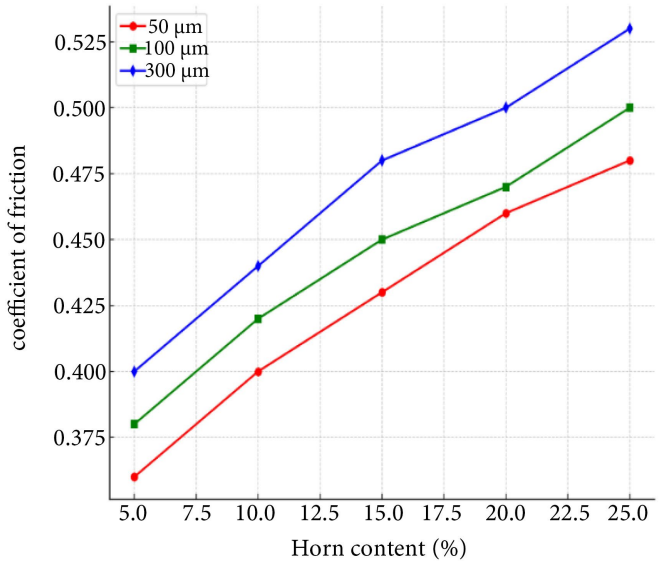

Figure 29. Change in the coefficient of friction as a function of horn content and particle size.

The graph above compares the change in the coefficient of friction for different horn particle sizes (50 µm, 100 µm, and 300 µm) as a function of horn content

(%). Regardless of the particle size, the coefficient of friction increases with horn content. This indicates that the bovine horn particles improve the composite's grip and slip resistance. Fine particles (50 μm) result in a lower coefficient of friction, reaching 0.48 for a horn content of 25%. Medium particles (100 μm) result in intermediate behavior, with a maximum value of 0.50. Coarse particles (300 μm) exhibit the highest coefficient of friction, 0.53, indicating better interaction with the friction surface. An increase in particle size leads to an increase in the coefficient of friction. This may be due to better interconnection of coarse particles, which increases surface roughness and slip resistance. However, particles that are too large can also accelerate material wear, requiring a compromise in the composite formulation. To better evaluate the performance of the ox horn and phenolic resin composite, we will compare its coefficient of friction with that of other materials used in braking and traction applications. Table 14 shows a comparison of coefficients of friction (100 μm particle size) with other composites.

Table 14. Comparison of coefficients of friction (100 μm particle size) with other composites.

Material	Static coefficient of friction	Dynamic coefficient of friction	References
Horn + Phenolic Resin Composite (100 μm)	0.42 to 0.50	0.40 to 0.47	Present study
Kevlar-based brake linings	0.35 to 0.45	0.30 to 0.40	[34]
Carbon fiber-based linings	0.40 to 0.55	0.38 to 0.50	[35]
Ceramic composite material (CCM)	0.45 to 0.60	0.40 to 0.55	[36]
Sintered metallic materials	0.30 to 0.40	0.25 to 0.38	[37]

The horn particle and phenolic resin composite has a coefficient of friction comparable to Kevlar and carbon fiber linings, making it a promising material for braking applications. However, it is slightly inferior to ceramic composite materials (CCMs), which are known for their exceptional thermal and tribological properties. Compared to sintered metal materials, it offers better grip but may be more susceptible to wear. This composite has a more stable coefficient of friction than wood and phenolic resin composites, but remains inferior to Kevlar and carbon fiber composites in terms of thermal stability and friction resistance [38] [39].

The initial phase (0 to 1,000 cycles) shows an increase in friction due to running-in. The stable phase (1,000 to 8,000 cycles) shows a stabilization of friction, indicating good tribological compatibility, while the final phase (8,000 to 10,000 cycles) highlights a slight decrease in friction, indicating the onset of wear. The optimal horn particle content is 15% to 20%, with a particle size of 100 μm, to ensure stability.

Slight variations around an average value of 0.3 suggest stability with minor fluctuations (see Figure 30). These fluctuations can be attributed to temperature

variations, changes in the contact surface, or tribological phenomena related to the composite material. An initial increase followed by stabilization may be due to the formation of a transfer film or gradual wear of the material.

Comparison with other composites [40] [41]: Study of the stability of the coefficient of friction of phenolic composites [42] [43]. The Kevlar + phenolic resin composite has excellent friction stability, but its production cost is high. The carbon fiber + phenolic resin composite also offers very good stability, but its coefficient of friction is relatively low, which may limit its use in certain braking applications. On the other hand, the wood + phenolic resin composite exhibits rapid wear and friction instability, which makes it unsuitable for applications requiring constant mechanical performance.

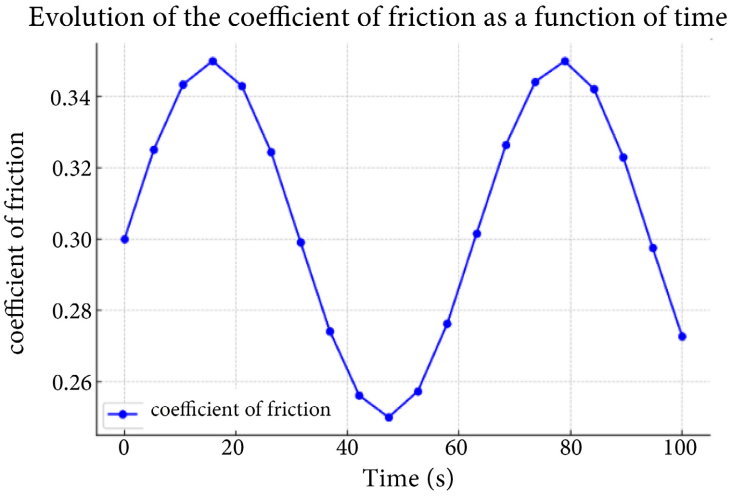

Figure 30. Evolution of the coefficient of friction over time.

3.2.5. Comparative Analysis: Phenolic Resin, Horn Composites, and Commercial Brake Lining

This analysis compares the thermomechanical properties of ox horn composites reinforced with phenolic resin, pure phenolic resin, and a commercial brake lining. The properties studied include Rockwell hardness and coefficient of friction, as a function of horn particle content and particle size.

The experimental data come from tests conducted on composites with different horn particle contents (5%, 10%, 15%, 20% and 25%) and three particle sizes (50 μm, 100 μm, 300 μm). Results for pure phenolic resin and a commercial brake lining are included for comparison.

Figure 31 below illustrates the variation in Rockwell hardness and coefficient of friction.

The results show a notable improvement in mechanical and tribological properties with the addition of horn particles. Rockwell hardness increases significantly compared to pure phenolic resin, especially for fine particles (50 μm). The coefficient of friction follows a similar trend, reaching values close to those of commercial lining at 20% - 25% horn content, indicating a marked strengthening effect.

The inclusion of horn particles simultaneously improves mechanical strength and tribological performance. Contents of 20% - 25% with 50 µm particles appear to offer the best compromise, bringing the composite's performance closer to that of commercial linings.

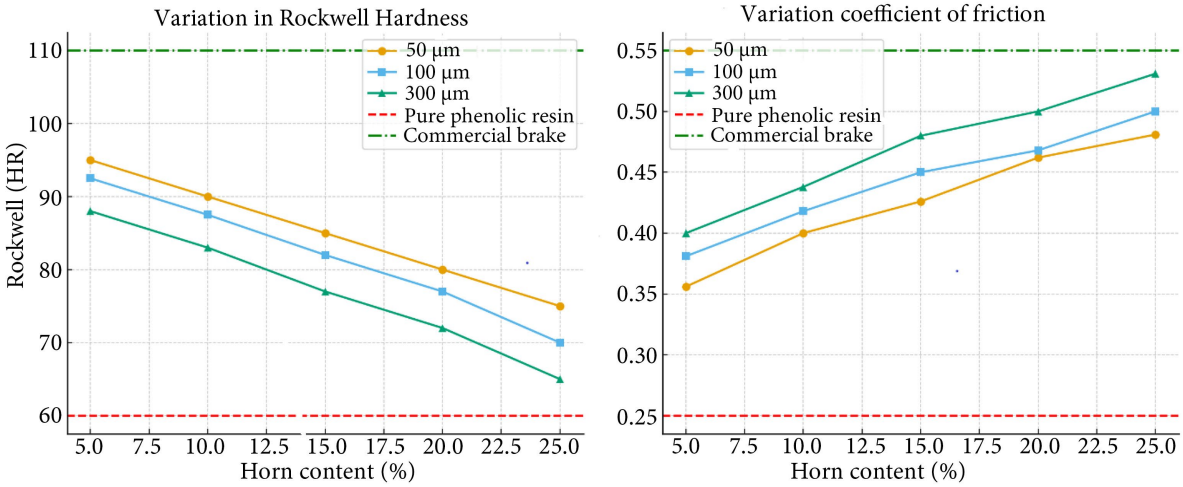

Figure 31. Comparative analysis illustrating the variation in Rockwell hardness and coefficient of friction: Phenolic resin, horn-based composites, and commercial lining.

3.2.6. Composite Wear Study and Specific Wear Analysis

The specific wear curve as a function of horn content is shown in the graph below.

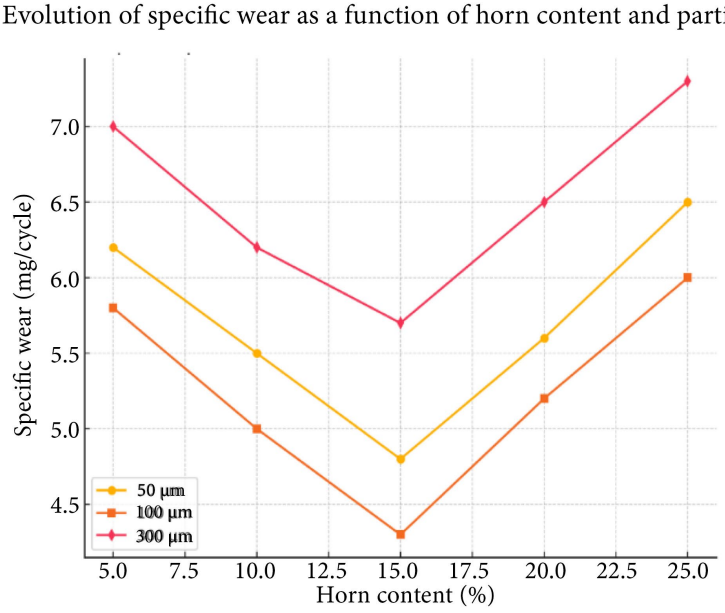

Figure 32. Specific wear as a function of horn content and particle size.

Figure 32 shows the specific wear as a function of horn content and particle size. Specific wear generally decreases with increasing horn content up to 15%,

then increases slightly. Composites containing 100 µm particles exhibit the lowest specific wear, suggesting an optimal balance between mechanical strength and tribological stability. 50 µm particles exhibit slightly higher wear than 100 µm particles, but remain higher than 300 µm particles. The latter exhibit greater wear, likely due to lower dispersion and reduced adhesion to the matrix. Composites containing 100 µm particles and 10% - 15% horn content offer the best wear resistance. Excessive horn content or particles that are too large impair the tribological performance of the material. Comparison with other materials reveals that the specific wear of carbon fiber and phenolic resin composites is generally lower (about 3 - 4 mg/cycle, according to [44]. They exhibit better mechanical strength, but higher cost. Natural fiber composites (e.g., hemp, flax) have similar specific wear as ox horn composites (about 4 - 6 mg/cycle according to [45]. They exhibit better biodegradability, but lower thermal resistance. Kevlar and phenolic resin composites have much lower specific wear (about 2 - 3 mg/cycle, according to [46]. They exhibit excellent wear resistance, but higher manufacturing cost and complexity. Ox horn and phenolic resin composite demonstrates good tribological performance for intermediate particle sizes (100 µm). It is between natural and advanced synthetic composites in terms of wear resistance. Its advantages are its lower cost and its biodegradability compared to synthetic alternatives. The best wear resistance is achieved with a horn particle content of 20% and 100 µm particles. The ox horn and phenolic resin composite exhibits better wear resistance than a wood and phenolic resin composite, but remains inferior to a Kevlar and phenolic resin composite [47] [48].

3.2.7. Thermal Resistance Study

Table 15 presents the results of thermal analysis of the different particles. The glass transition temperature (Tg) is higher for 100 µm particles, indicating better cohesion. The degradation temperature is more stable at 100 µm. Thermal degradation and mass loss are greater for particles that are too large (300 µm). The DSC (differential scanning calorimetry) analysis curve of various composites is shown in Figure 33.

The glass transition (Tg) is detected at 220˚C for 50 µm particles; 230˚C for 100 µm particles; and 215˚C for 300 µm particles. The sample containing 100 µm particles exhibits the most pronounced transition, suggesting stronger adhesion between the resin and the horn particles. Figure 34 presents the TGA curves of the composites with different particle sizes.

Table 15. Thermal analysis of the different particles.

Particle size (µm)	Tg (˚C) Thermal	Degradation TGA (˚C)	Mass loss at 600˚C (%)
50	220	350	35
100	230	370	30
300	215	340	40

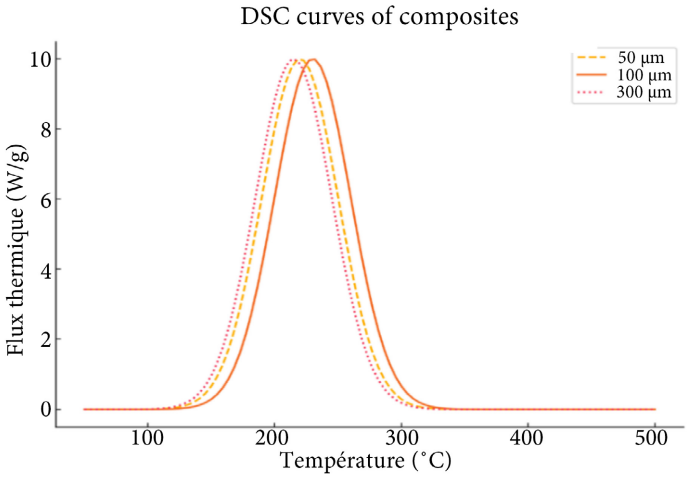

Figure 33. DSC curve of different particle sizes.

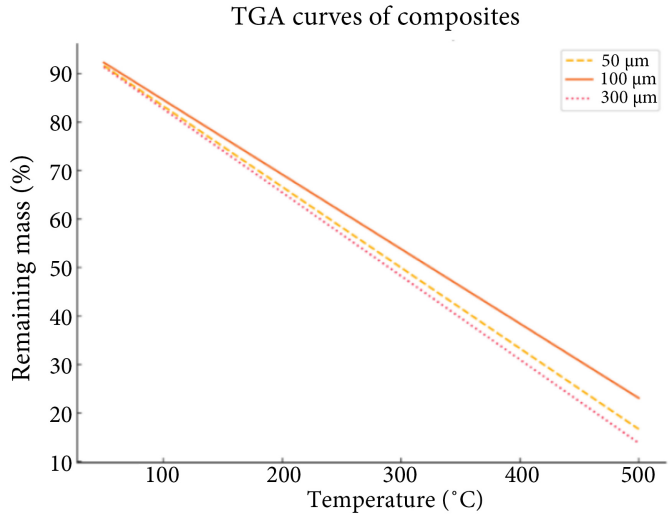

Figure 34. TGA curves of composites with different particle sizes.

Table 16. Comparison of thermal resistance (ATG and DSC) with other materials.

Material	Degradation Temperature (TGA ˚C)	Glass Transition (DSC ˚C)
Ox horn composite + phenolic resin (100 µm)	370	230
Carbon fiber composite + phenolic resin	400	250
Kevlar composite + phenolic resin	380	240
Wood powder composite + phenolic resin	320	200

Thermal degradation begins around 350˚C for 50 µm particles. It is slightly delayed for 100 µm particles (around 370˚C), confirming their better thermal stability. 300 µm particles degrade at a lower temperature (around 340˚C), probably due to uneven

charge distribution. 100 µm particles offer the best compromise between thermal and mechanical strength. Composites containing 300 µm particles perform less well, probably due to less homogeneity of the material. This material is particularly suitable for braking and anti-wear coating applications (see Table 16).

Carbon fiber and Kevlar composites offer better thermal stability than ox horn composites. Wood/phenolic resin composites are less thermally resistant, confirming that ox horn offers a good compromise.

Table 17: Comparison of ox horn + phenolic resin composite with other materials. Carbon fiber and Kevlar composites offer better thermal stability than ox horn composites. Wood/phenolic resin composites are less thermally resistant, confirming that ox horn offers a good compromise.

Table 17. Comparison of ox horn + phenolic resin composite with other materials.

Composite Property	Ox horn + phenolic resin	Kevlar + phenolic resin	Carbon fiber + phenolic resin	Wood + phenolic resin
Specific wear (mm^3/Nm)	2.5 to 3.0	1.5 to 2.0	1.0 to 1.8	3.5 to 4.5
Coefficient of friction	0.35 to 0.45	0.4 to 0.5	0.3 to 0.4	0.25 to 0.35
Decomposition temperature (˚C)	450	500	550	350
Tg (˚C)	220	250	300	180
Density (g/cm^3)	1.2 to 1.4	1.4 to 1.6	1.5 to 1.8	1.0 to1.2
Cost (€/kg)	5 to 7	20 to 30	25 to 40	2 to 5

The advantages of the composite made from ox horn particles and phenolic resin are good wear resistance (see Table 18), low cost, and biodegradability. It also has good thermal resistance (better than wood, but inferior to synthetic fibers). However, its performance is inferior to that of carbon or Kevlar fibers in some respects, but could be improved by adding mineral fillers (SiC, Al_2O_3).

Table 18. Areas of application.

Application	Recommended material
Brake pads	Ox horn + phenolic resin (good wear resistance and thermal stability)
Protective coatings	Kevlar + phenolic resin (better impact resistance)
Lightweight structural parts	Carbon fiber + phenolic resin (high rigidity and thermal resistance)
Thermal insulation materials	Wood + phenolic resin (low cost, good insulation)

4. Conclusion

This study demonstrates that a composite material formulated from ox horn particles and phenolic resin, particularly with a particle size of 100 µm, offers a satis-

factory compromise between thermal resistance, mechanical strength, and accessibility. Although its performance does not reach the levels of high-end materials such as carbon fibers or Kevlar, it remains a promising eco-friendly alternative for moderate-friction applications, including brake linings, protective panels, or insulating coatings. The results highlight that particle size and filler content are key parameters influencing hardness, thermal stability, and friction behavior. Ox horn, a natural protein-based filler, contributes to material reinforcement while reducing reliance on synthetic components. However, to further improve thermo-mechanical performance, future formulations could incorporate mineral fibers (such as SiO_2 or Al_2O_3) to enhance thermal stability and wear resistance. Similarly, the integration of natural reinforcements such as basalt or hemp fibers could help maintain a fully bio-sourced profile while increasing structural integrity. A few limitations can affect the long-term braking performance of composites. Moisture absorption can lead to matrix swelling, material softening, and reduced interfacial adhesion. Similarly, the presence of open porosity can accelerate crack initiation and propagation under repeated thermal and mechanical stresses. In addition, particle agglomeration can lead to inhomogeneous load distribution, resulting in localized wear and reduced friction layer stability. All of these factors can compromise the durability and reliability of the braking system during prolonged use. Overall, this research confirms the technical feasibility and potential of ox horn-based composites in the field of friction materials, provided they are properly designed and hybridized for the desired level of performance.

Conflicts of Interest

The authors declare no conflicts of interest regarding the publication of this paper.

References

[1] Wu, X. and Zhu, Y. (2021) Heterogeneous Materials: A New Class of Materials with Unprecedented Mechanical Properties. In: Wu, X.L. and Zhu, Y.T., Eds., *Heterostructured Materials*, Jenny Stanford Publishing, 3-16. https://doi.org/10.1201/9781003153078-2

[2] Saravanan, D., Sollapur, S.B., Anjappa, S.B., Malla, C., Satya Prasad, M. and Vignesh, S. (2022) Tribological Properties of Filler and Green Filler Reinforced Polymer Composites. *Materials Today*: *Proceedings*, **50**, 2065-2072. https://doi.org/10.1016/j.matpr.2021.09.414

[3] Milosevic, M., Valášek, P. and Ruggiero, A. (2020) Tribology of Natural Fibers Composite Materials: An Overview. *Lubricants*, **8**, Article 42. https://doi.org/10.3390/lubricants8040042

[4] Bai, H., Zhong, L., Kang, L., Liu, J., Zhuang, W., Lv, Z., *et al.* (2021) A Review on Wear-Resistant Coating with High Hardness and High Toughness on the Surface of Titanium Alloy. *Journal of Alloys and Compounds*, **882**, Article ID: 160645. https://doi.org/10.1016/j.jallcom.2021.160645

[5] Zhong, Z. (2021) Processes for Environmentally Friendly and/or Cost-Effective Manufacturing. *Materials and Manufacturing Processes*, **36**, 987-1009. https://doi.org/10.1080/10426914.2021.1885709

[6] Yang, F., Das, D., Karunakaran, K., Genin, G.M., Thomopoulos, S. and Chasiotis, I. (2023) Nonlinear Time-Dependent Mechanical Behavior of Mammalian Collagen Fibrils. *Acta Biomaterialia*, **163**, 63-77. https://doi.org/10.1016/j.actbio.2022.03.005

[7] Reiche, A., Dohme-Meier, F. and Claudia Terlouw, E.M. (2020) Effects of Horn Status on Behaviour in Fattening Cattle in the Field and during Reactivity Tests. *Applied Animal Behaviour Science*, **231**, Article ID: 105081. https://doi.org/10.1016/j.applanim.2020.105081

[8] Huang, W., Zaheri, A., Jung, J., Espinosa, H.D. and Mckittrick, J. (2017) Hierarchical Structure and Compressive Deformation Mechanisms of Bighorn Sheep (*Ovis canadensis*) Horn. *Acta Biomaterialia*, **64**, 1-14. https://doi.org/10.1016/j.actbio.2017.09.043

[9] Li, B.W., Zhao, H.P., Feng, X.Q., Guo, W.W. and Shan, S.C. (2010) Experimental Study on the Mechanical Properties of the Horn Sheaths from Cattle. *Journal of Experimental Biology*, **213**, 479-486. https://doi.org/10.1242/jeb.035428

[10] Alyanak, E. (2025) Exploring Expert and Stakeholders Beliefs on the Role, Evolution, and Future of the Advisory Committee on Immunization Practices. Ph.D. Thesis, The George Washington University.

[11] Ilie, F. and Cristescu, A. (2022) Tribological Behavior of Friction Materials of a Disk-Brake Pad Braking System Affected by Structural Changes—A Review. *Materials*, **15**, Article 4745. https://doi.org/10.3390/ma15144745

[12] Muraliraja, R., Tamilarasan, T.R., Udayakumar, S. and Arvinda Pandian, C.K. (2020) The Effect of Fillers on the Tribological Properties of Composites. In: Hameed Sultan, M.T., Mohd Jamir, M.R., Abdul Majid, M.S., Azmi, A.I. and Saba, N., Eds., Tribological Applications of Composite Materials, Springer, 243-266. https://doi.org/10.1007/978-981-15-9635-3_9

[13] Tawe, L., Gaga, D.B., Zakary, Y., Karga, T.L. and Danwe, R. (2022) Mechanical Behaviours of Composite Material Manufactured with Beef Horn Sheath's Adhesives. *American Journal of Engineering Research* (*AJER*), **11**, 48-53. https://www.ajer.org/papers/Vol-11-issue-1/H11014853.pdf

[14] Oh, E., Godoy Zúniga, M.M., Nguyen, T.B., Kim, B., Trung Tien, T. and Suhr, J. (2024) Sustainable Green Composite Materials in the Next-Generation Mobility Industry: Review and Prospective. *Advanced Composite Materials*, **33**, 1368-1419. https://doi.org/10.1080/09243046.2024.2348237

[15] Hadian, M., Marrevee, D.P.F., Buist, K.A., Reesink, B.H., Bos, A.N.R., Bavel, A.P., *et al.* (2022) Kinetic Study of Thermocatalytic Decomposition of Methane over Nickel Supported Catalyst in a Fluidized Bed Reactor. *Chemical Engineering Science*, **260**, Article ID: 117938. https://doi.org/10.1016/j.ces.2022.117938

[16] Zhai, W., Bai, L., Zhou, R., Fan, X., Kang, G., Liu, Y., *et al.* (2021) Recent Progress on Wear-Resistant Materials: Designs, Properties, and Applications. *Advanced Science*, **8**, Article ID: 2003739. https://doi.org/10.1002/advs.202003739

[17] Onukwuli, O.D. and Ezeh, E.M. (2021) Assessment of the Fire Retardant Effect Potential of Carbonized Cow Horn Ash Additive in Banana Peduncle Fibre Reinforced Polyester Composites. *World Journal of Engineering*, **20**, 399-408. https://doi.org/10.1108/wje-07-2021-0438

[18] Meyers, R.A. (2020) Encyclopedia of Analytical Chemistry: Applications, Theory and Instrumentation. John Wiley & Sons.

[19] Park, S., Kang, M., Oinam, Y., Amoozegar, A. and Pyo, S. (2022) Measurement of Skeletal Density and Porosity of Construction Materials Using a New Proposed Vac-

uum Pycnometer. *Measurement*, **196**, Article ID: 111209. https://doi.org/10.1016/j.measurement.2022.111209

[20] Lavaggi, T., Muhammed, F., Moretti, L., Gillespie, J.W. and Advani, S.G. (2024) Correlation of the Permeability and Porosity Development of Carbon/Carbon Composites during Pyrolysis. *Composites Part A*: *Applied Science and Manufacturing*, **181**, Article ID: 108156. https://doi.org/10.1016/j.compositesa.2024.108156

[21] Marchoubeh, M.L., Knight, H. and Horn, G.P. (2024) A Pyrolysis-Gas Chromatography/Mass Spectrometry Study of Volatile Compounds Produced by Wood-Based Materials. *Fire and Materials*, **48**, 542-550. https://doi.org/10.1002/fam.3202

[22] Zemene, F. (2024) Experimental Investigation on Mechanicalproperties of Hybrid Polymer Composite Made from HDPE Reinforced with Cow Bone and Hornparticles for Door Panel Applications. Ph.D. Thesis, University of Gondar.

[23] Ezeh, C.I., Onukwuli, O.D. and Mbah, G.C. (2020) Physicochemical Characterization of Cow Horn Ash and Its Effect as Filler Material on the Mechanical Property of Polyester-Banana Peduncle Fibre Composites. *World Journal of Engineering*, **17**, 823-829. https://doi.org/10.1108/WJE-08-2020-0351

[24] Huang, J., Chen, H., Yang, J., Zhou, T. and Zhang, H. (2023) Effects of Particle Size on Microstructure and Mechanical Strength of a Fly Ash Based Ceramic Membrane. *Ceramics International*, **49**, 15655-15664. https://doi.org/10.1016/j.ceramint.2023.01.157

[25] Liu, G., Zhang, C., Zhao, M., Guo, W. and Luo, Q. (2020) Comparison of Nanomaterials with Other Unconventional Materials Used as Additives for Soil Improvement in the Context of Sustainable Development: A Review. *Nanomaterials*, **11**, Article 15. https://doi.org/10.3390/nano11010015

[26] Cai, M., Zhu, H., Rabczuk, T. and Zhuang, X. (2025) Mixer Influence on Pore Characteristics and Fiber Dispersion in Engineered Cementitious Composites across Various Strength Grades. *Construction and Building Materials*, **467**, Article ID: 140380. https://doi.org/10.1016/j.conbuildmat.2025.140380

[27] Zhou, X., Liu, S., Siddique, A., Min, C., Pei, X., Liu, S., *et al.* (2025) Construction of Nanocomposite Interphase with Controllable Thickness to Relieve Stress Concentration and Boost Stress Transfer from Carbon Fiber/epoxy Resin Interface. *Chemical Engineering Journal*, **505**, Article ID: 159542. https://doi.org/10.1016/j.cej.2025.159542

[28] Megahed, M., Fathy, A., Morsy, D. and Shehata, F. (2019) Mechanical Performance of Glass/Epoxy Composites Enhanced by Micro- and Nanosized Aluminum Particles. *Journal of Industrial Textiles*, **51**, 68-92. https://doi.org/10.1177/1528083719874479

[29] Khan, A.A., Zafar, M.S., Ali A Ghubayri, A., AlMufareh, N.A., Binobaid, A., Eskandrani, R.M., *et al.* (2020) Polymerisation of Restorative Dental Composites: Influence on Physical, Mechanical and Chemical Properties at Various Setting Depths. *Materials Technology*, **37**, 2056-2062. https://doi.org/10.1080/10667857.2020.1837555

[30] Priyanka, P., Mali, H.S. and Dixit, A. (2023) Carbon-Kevlar Intraply Hybrid Fabric Polymer Composites: Mechanical Performance. *Iranian Polymer Journal*, **32**, 633-645. https://doi.org/10.1007/s13726-023-01150-3

[31] Ursache, Ş., Cerbu, C. and Hadăr, A. (2023) Characteristics of Carbon and Kevlar Fibres, Their Composites and Structural Applications in Civil Engineering—A Review. *Polymers*, **16**, Article 127. https://doi.org/10.3390/polym16010127

[32] Zuska, A., Kurczyński, D. and Jackowski, J.T. (2023) Study of Loads Acting on the

Load during the Sudden Braking of a Vehicle. *Applied Sciences*, **13**, Article 1559. https://doi.org/10.3390/app13031559

[33] Li, C., Zhuo, G., Tang, C., Xiong, L., Tian, W., Qiao, L., *et al.* (2023) A Review of Electro-Mechanical Brake (EMB) System: Structure, Control and Application. *Sustainability*, **15**, Article 4514. https://doi.org/10.3390/su15054514

[34] Kumar, N., Grewal, J.S., Singh, A. and Mehta, V. (2021) A Comparative Study of Alkali Treated Date Palm Fiber Based Brake Friction Composites and Standard Kevlar-based Brake Friction Composites. *Polymer Composites*, **43**, 239-249. https://doi.org/10.1002/pc.26370

[35] Monazami, M. (2023) Multiphase Characteristics of Carbon Fiber-Reinforced Cementitious Materials Under Static and Freeze-Thaw Cyclic Loading Conditions. Ph.D. Thesis.

[36] Oliveira, T.L.L. (2021) Federal University of Itjauba.

[37] Jain, H., Shadangi, Y., Chakravarty, D., Dubey, A.K. and Mukhopadhyay, N.K. (2022) High Entropy Steel Processed through Mechanical Alloying and Spark Plasma Sintering: Alloying Behaviour, Thermal Stability and Mechanical Properties. *Materials Science and Engineering*: *A*, **856**, Article ID: 144029. https://doi.org/10.1016/j.msea.2022.144029

[38] Maiti, S., Islam, M.R., Uddin, M.A., Afroj, S., Eichhorn, S.J. and Karim, N. (2022) Sustainable Fiber-Reinforced Composites: A Review. *Advanced Sustainable Systems*, **6**, Article ID: 2200258. https://doi.org/10.1002/adsu.202200258

[39] Kamarudin, S.H., Mohd Basri, M.S., Rayung, M., Abu, F., Ahmad, S., Norizan, M.N., *et al.* (2022) A Review on Natural Fiber Reinforced Polymer Composites (NFRPC) for Sustainable Industrial Applications. *Polymers*, **14**, Article 3698. https://doi.org/10.3390/polym14173698

[40] Padhan, M., Marathe, U. and Bijwe, J. (2020) Surface Topography Modification, Film Transfer and Wear Mechanism for Fibre Reinforced Polymer Composites—An Overview. *Surface Topography*: *Metrology and Properties*, **8**, Article ID: 043002. https://doi.org/10.1088/2051-672x/abbcb6

[41] Panin, S.V., Alexenko, V.O. and Buslovich, D.G. (2022) High Performance Polymer Composites: A Role of Transfer Films in Ensuring Tribological Properties—A Review. *Polymers*, **14**, Article 975. https://doi.org/10.3390/polym14050975

[42] Zhang, E., Gao, F., Fu, R., Lu, Y., Han, X. and Su, L. (2021) Tribological Behavior of Phenolic Resin-Based Friction Composites Filled with Graphite. *Materials*, **14**, Article 742. https://doi.org/10.3390/ma14040742

[43] Patnaik, A., Kumar, M., Satapathy, B.K. and Tomar, B.S. (2010) Performance Sensitivity of Hybrid Phenolic Composites in Friction Braking: Effect of Ceramic and Aramid Fibre Combination. *Wear*, **269**, 891-899. https://doi.org/10.1016/j.wear.2010.08.023

[44] Niu, Z., Chen, F., Xiao, P., Li, Z., Pang, L. and Li, Y. (2021) Effect of h-BN Addition on Friction and Wear Properties of C/C-SiC Composites Fabricated by LSI. *International Journal of Applied Ceramic Technology*, **19**, 108-118. https://doi.org/10.1111/ijac.13838

[45] Lang, S.Q., *et al.* (2025) Site U1601. *Proceedings of the International Ocean Discovery Program*, **399**, 399.

[46] Tang, H., Li, P., Li, Z., Li, J., Zhao, J., Xu, Y., *et al.* (2022) Braking Behaviours of C/C-SiC Mated with Iron/Copper-Based PM in Dry, Wet and Salt Fog Conditions. *Ceramics International*, **48**, 3261-3273. https://doi.org/10.1016/j.ceramint.2021.10.100

[47] Ismail, A.S., Jawaid, M., Zainudin, E.S., Yahaya, R., Alothman, O.Y., Abu-Jdayil, B., *et al.* (2025) Dimensional Stability, Mechanical and Thermal Performance of Flax/Carbon/Kevlar Reinforced Bio-Phenolic/Epoxy Hybrid Composites. *Journal of Natural Fibers*, **22**, Article ID: 2461491. https://doi.org/10.1080/15440478.2025.2461491

[48] Krishnasamy, S., Ramachandran, S., Swaminathan, G., Thirukumaran, M., Hema, M., Parameswaranpillai, J., *et al.* (2024) Hybrid Glass/Kevlar Fiber Reinforced Phenolic Matrix Composites: Thermal Degradation and Flammability Studies. *Polymer Composites*, **46**, 7108-7119. https://doi.org/10.1002/pc.29416